CHARLES UNIVERSITY

Faculty of Science

Department of Biochemistry

Bc. Ján Sabó

Impact of membrane properties on clustering of transmembrane peptides

Vliv membránových vlastností na shlukování transmembránových peptidů

Diploma thesis

Supervisor: Mgr. Marek Cebecauer, Ph.D.

Consultant: RNDr. Petr Novák, Ph.D.

Praha, 2019

Declaration

Hereby I declare that I worked on the thesis independently, under supervision of Mgr. Marek Cebecauer, Ph.D. and RNDr. Peter Novák, Ph.D. and all the sources where properly cited. Neither this thesis nor its considerable part has been submitted to claim different or similar academic title.

Prohlašuji, že jsem závěrečnou práci zpracoval samostatně pod odborným vedením Mgr. Marka Cebecauera, Ph.D. a RNDr. Petra Nováka, Ph.D. a všechny použité prameny jsem řádně citoval. Tato práce ani její podstatná část nebyla předložená k získání jiného nebo stejného akademického titulu.

In Prague/V Praze ……....

……

Bc. Ján Sabó

Acknowledgement

I would like to thank my supervisor Mgr. Marek Cebecauer, Ph.D. and my consultant RNDr. Petr Novák, Ph.D. for helpful advices throughout my work on this thesis.

Many thanks to Mgr. Zdeněk Kukačka, PhD. for mass spectrometry analysis.

Big thank you belongs to the whole Department of Biophysical Chemistry at the UFCH-JH, AV ČR for perfect working environment and immediate aid when needed. Special thanks for technical help at the beginning of the thesis to Mgr. Jan Sýkora, PhD. and Dr. Peter Kapusta.

At last, I would like to thank my family for help and support throughout my studies.

Abstract

Unfolded protein response (UPR) is a complex cellular mechanism induced upon ER stress caused by various environmental factors. Single spanning signal transducers of UPR were reported to recognise also lipid-induced ER stress. Studies of these transducers, namely PERK and IRE1 uncovered that they can sense change in membrane properties and activate themselves by clustering. Moreover, signal transducer IRE1 retained ability to sense changes in the membrane properties with TMD exchanged for a polyLeu α-helix. It was thus unclear what mechanism drives lipid-induced UPR via IRE1. We employed model membrane system in form of LUVs, where properties of membranes can be readily altered by specific lipid composition. As a simplified model of the UPR signal transducers in the ER, synthetic transmembrane peptides with polyLeu core were used. Dynamic light scattering (DLS) has been used for qualitative and semi-quantitative analysis of LUVs. Clustering of synthetic peptides was determined by time resolved anisotropy of fluorescence.

DLS results demonstrate successful formation of vesicles with a desired size in all planned composition. On the contrary to the studies in living cells, the presence of cholesterol or palmitic acid in model membranes did not induce the aggregation of transmembrane peptides. However, the formation of peptide clusters was observed under the conditions of negative hydrophobic mismatch or a very high membrane rigidity. The most noticeable change in the aggregation of peptides was detected when a charge of their flanking residues was altered. In summary, we show that the used method is suitable for recognition of peptide clustering in model membranes. Current results also indicate the importance of a net charge of flanking residues as a factor in molecular mechanism which may contribute to the activation of ER stress sensors.

Key words: liposomes, synthetic transmembrane peptides, clustering, fluorescence spectroscopy

Abstrakt

Odpověď na chybně sbalené proteiny (dále jen UPR, z angl. „unfolded protein response“) je komplexní buněčný mechanizmus vyvolaný v reakci na stres endoplasmatického retikula (dále jen ER), který může být způsoben různými faktory. Proteinové přenašeče signálu UPR, které jsou zakotveny do membrány ER pomocí jednoho α-helixu, mohou rozpoznat také stres ER indukovaný lipidy. Studie těchto přenašečů signálu UPR, zejména PERK a IRE1, poukazují na schopnost přenašečů rozlišovat změny ve vlastnostech membrány ER tvorbou agregátů a tím se aktivovat. Schopnost proteinu IRE1 rozeznat změnu v membránových vlastnostech včetně jeho následné aktivace byla zachována i v mutantu, kde nativní transmembránová doména byla zaměněna za polyLeu α-helix. Mechanizmus aktivace proteinu IRE1 během lipidy indukované UPR ale nebyl objasněn. Ke studiu chování proteinů v membránách jsme použili modelové lipidové membrány ve formě vezikul (liposomy), ve kterých lze jednoduše měnit membránové vlastnosti změnou lipidového složení. Jako zjednodušený model přenašeče signálu UPR v ER byl použit syntetický transmembránový peptid s polyLeu jádrem. Pro kvalitativní a semi-kvantitativní analýzu liposomů byla použita metoda dynamického rozptylu světla (DLS, z angl. „dynamic light scattering“). Tvorba agregátů syntetických peptidů v membránách liposomů byla určena pomocí časově rozlišené anizotropie fluorescence.

Výsledky získané metodou DLS poukazují na úspěšnou tvorbu liposomů s požadovanou velikostí ve všech testovaných složeních modelových membrán. V porovnání se studiemi na živých buňkách, přítomnost cholesterolu a palmitátu v modelových membránách neindukovala tvorbu peptidových agregátů. Transmembránové peptidy ale vytvářeli klastry v přítomnosti negativního hydrofobního rozdílu nebo v modelových membránách s vysokou rigiditou. Nejvýraznější změna v agregaci peptidů byla zaznamenána u peptidů s rozdílným nábojem aminokyselin na okrajích hydrofobního jádra transmembránového peptidu. V této práci jsme ukázali, že metodu časově rozlišené anizotropie fluorescence lze využít k detekci peptidových agregátů v modelových membránách. Výsledky této práce dále poukazují na důležitost celkového náboje v sekvencích aminokyselin v blízkosti transmembránové domény proteinů. Tento faktor by mohl přispívat k molekulárnímu mechanizmu aktivace senzorů stresu ER.

Klíčová slova: liposomy, syntetické transmembránové peptidy, tvorba klastrů, fluorescenční spektroskopie

Table of content

List of used symbols and abbreviations

24:1PC	1,2-dinervonyl-sn-glycero-3-phosphocholine
ATF6	activating transcription factor 6
DLS	dynamic light scattering
DOPC	1,2-dioleyl-sn-glycero-3-phosphocholine
DPPC	1,2-dipalmitoyl-sn-glycero-3-phosphocholine
CHOL	cholesterol
CSSR	core stress sensing region
ER	endoplasmic reticulum
ERAD	endoplasmic-reticulum-associated protein degradation
FRET	Förster resonance energy transfer
IRE1	inositol requiring 1 gene
homo-FRET	Förster resonance energy transfer between molecules of the same kind
LUV	large unilamellar vesicle
LW21	synthetic peptide with polyLeu core
MD	molecular dynamics
MiliQ	filtered Milipore water
MLV	multilamellar vesicle
MS	mass spectrometry
PA	palmitic acid
PC	phosphatidylcholine
PERK	double-stranded RNA-activated protein kinase (PKR)–like ER kinase
PdI	polydispersity index
PGPC	1-palmitoyl-2-glutaryl-sn-glycero-3-phosphocholine
POPC	1-palmitoyl-2-oleoyl-sn-glycero-3-phosphocholine
TCSPC	time-correlated single photon counting
TFE	2,2,2-trifluoroethanol
TMD	transmembrane domain
UPR	unfolded protein response
VBA	visual basic for application
VH	perpendicular relative orientation of excitation and emission polarizers
VV	parallel relative orientation of excitation and emission polarizers

1 Introduction

Biological membranes are necessary for life existence as we know it[1]. In addition to their role in protecting cells from their surrounding environment, they compartmentalise internal volume of the cell into smaller sections – organelles, which may have specific function. Main components of biological membranes are lipids and proteins[2]. Current model of lipid and protein organisation in the membranes is the updated fluid mosaic model originally suggested by Singer and Nicolson in 1972[3,4]. It states that proteins are embedded into the lipid bilayer where they can diffuse in the membrane plane (**Fig. 1**). Embedded proteins provide membranes with a huge variability of functionalities: e.g. transport of molecules and its regulation, support for the cytoskeleton, signal transduction, catalysis of metabolic processes and many more. So, how is it possible that lipids and proteins form such a complex system with a vast functionality? To answer this question, we have to look at their biochemical composition and biophysical properties.

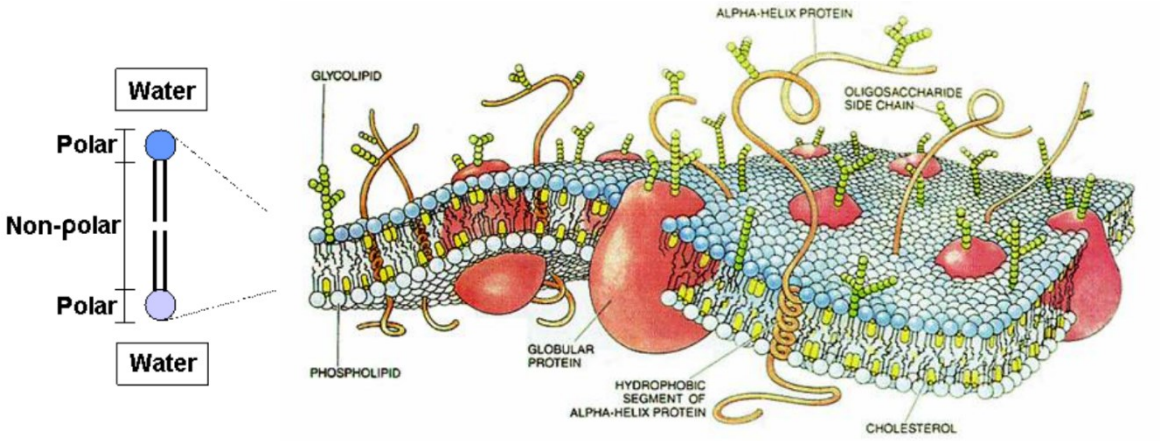

Fig. 1 Biological membrane separating two water phases. Scheme of polarity across the membrane (left). On the right-hand side, a schematic illustration of a biological membrane according to the fluid mosaic model containing phospholipids, glycolipids, cholesterol and glycosylated transmembrane proteins. Figure was adapted[5].

1.1 Biochemical and biophysical properties of membranes

When studying cellular processes in membranes, it is crucial to understand the properties that this organelle possesses. A unique biochemical composition of specific membrane components gives rise to a variety of biophysical properties. At first, biochemical properties of membrane lipids and proteins will be discussed separately, which is followed by more specific sections relevant to the thesis.

1.1.1 Membrane lipids

The most abundant molecular species in biological membranes are lipids, of which phospholipids form the largest part. They generally possess amphipathic properties that

allow for the spontaneous formation of a bilayer. A bilayer is formed by two layers of lipid molecules interacting together via hydrophobic tails and exposing their hydrophilic heads to the surrounding polar environment (**Fig. 1**, p. 9). Chemically, lipids are very variable and several types can be distinguished. Glycerophospholipids are the most abundant lipid species in biological membranes[6]. Their core is formed by 3-phosphoglycerol that has hydroxyl groups esterified by fatty acids (**Fig. 2A,** p. 11). Upon exchanging the substituents on the phosphate, different types of glycerophospholipids can be distinguished, such as phosphatidylcholine (PC) (**Fig. 2A,** p. 11), phosphatidylethanolamine, phosphatidylserine and phosphatidylinositol (**Fig. 2B,** p. 11). In membranes of plant cells, dominant lipid species are galactolipids [7]. These diacylglycerols contain galactose, that is bound onto glycerol via 1-hydroxyl group. These lipid species do not contain phosphate group. Sphingolipids also form a significant part of some cellular membranes, e.g. the plasma membrane of higher vertebrates[8]. Sphingosine, a long hydrophobic chain containing amino-alcohol forms a core of these lipids. In case that its amino group is substituted with a fatty acid, such molecules are classified as ceramides. Sphingolipids can be further divided. In case a polar headgroup is bound to the sphingosine, these are sphingomyelins (contain phosphocholine or phosphoethanolamine (**Fig. 2C,** p. 11)), cerebrosides (contain glycosidic bond to a sugar moiety) and gangliosides (their sugar moiety contains sialic acid). All the above-mentioned lipid molecules are "two legged", where "legs" are fatty acids connected to glycerol (**Fig. 2A,** p. 11) or, in case of sphingolipids, one of the "legs" is the aliphatic chain of sphingosine (**Fig. 2C,** p. 11). Considering the fatty acids, variability of lipid molecules increases immensely allowing membrane to adjust easily its composition in order to keep the homeostasis under everchanging conditions in living organisms. Examples of chemical structures of unsaturated (nervonic) and saturated fatty acids (palmitic) are depictured in **Fig. 2E** (p. 11). Oxidative stress can induce changes in phospholipid structure. Reactive oxygen species can disrupt double bonds on fatty acyl chains by formation of hydroxides or hydroperoxides[9]. In some cases, this leads to a truncation of phospholipid acyl chains and typically *sn*-2 position of phospholipid is occupied by shortened aldehyde or carboxylic acid (**Fig. 2E**, p. 11)[10].

Another crucial components of the eukaryotic membranes are sterols. Their chemical structure is derived from sterane (cyclopentanoperhydrophenanthrene) and play a role in the modification of membrane rigidity[11]. The best known and most studied sterol is cholesterol[12]. Distribution of polarity throughout its chemical structure exhibits some

similarity to amphipathic phospholipids, with the hydroxy group on C3 forming the polar head and the alkyl chain the hydrophobic part (**Fig. 2D**).

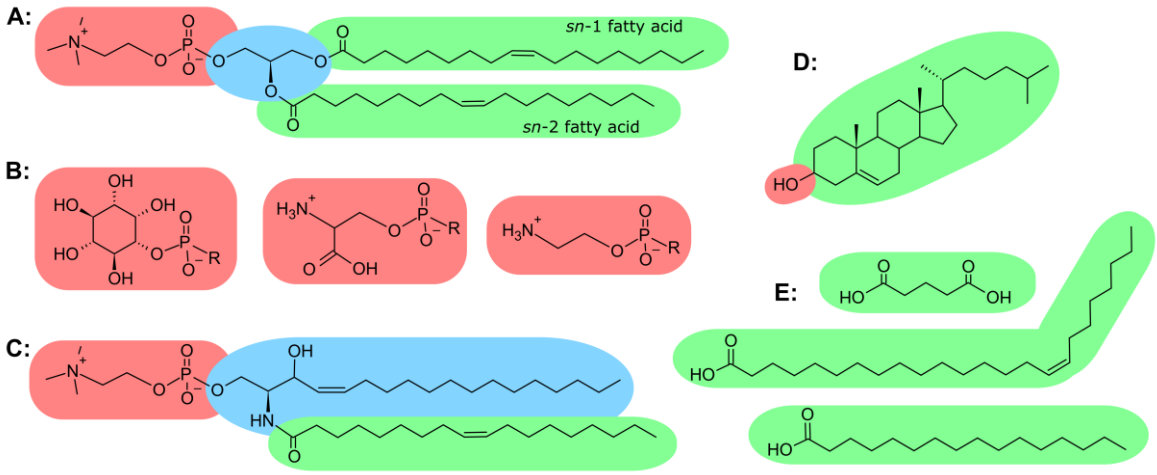

Fig. 2 Chemical structures of selected membrane lipids. A: Glycerophospholipid – dioleoyl phosphatidylcholine (DOPC). Highlighted parts: red – phosphocholine, blue – glycerol, green – oleic acids. **B:** Alternative phospholipid headgroups. Left to right: phosphatidylinositol, phosphatidylserine, phosphatidylethanolamine. **C:** Sphingomyelin: red – phosphocholine, blue – sphingosine, green – oleic acid. **D:** Chemical structure of cholesterol. Polar head group is highlighted in red. **E:** Examples of fatty acids that can covalently bind to glycerol or sphingosine. Top to bottom: glutaric acid (not a fatty acid, exists in oxidised lipids), nervonic acid and palmitic acid.

1.1.2 Membrane proteins

Proteins associated with membranes are responsible for functional variability of biological membranes. Numerous vital processes are executed in membranes that contain high mass percentage of proteins. They contribute to as much as 80 % of the inner mitochondrial membrane mass[13] and 50 % to both the thylakoid membrane of chloroplasts[14] and the plasma membrane[15].

The extent of the interaction between membranes and proteins can be used for the categorization of proteins. Two categories are distinguished: peripheral and integral membrane proteins[2]. Peripheral proteins can interact with the membrane reversibly upon post-translational modifications by phosphorylation or ligand binding (cyan in **Fig. 3**, p. 12)[16,17]. In other case, peripheral proteins have one or more surface amino acid functionalised by covalent bond to non-polar molecule that arranges their association with membranes (violet in **Fig. 3**, p. 12). The examples of these non-polar molecules are phospholipids (e.g. GPI-anchor), isoprenoids (e.g. farnesyl) or fatty acids (e.g. palmitic acid)[18]. The second group of membrane proteins are integral membrane proteins that span the thickness of biological membrane. Intramembrane part can be formed by a single[19] or multiple α-helices[20] with non-polar amino acids on its surface or by a β-barrel with a vacant

interior thus potentially forming pores[21]. The types of membrane spanning structures of protein are depicted in **Fig. 3**.

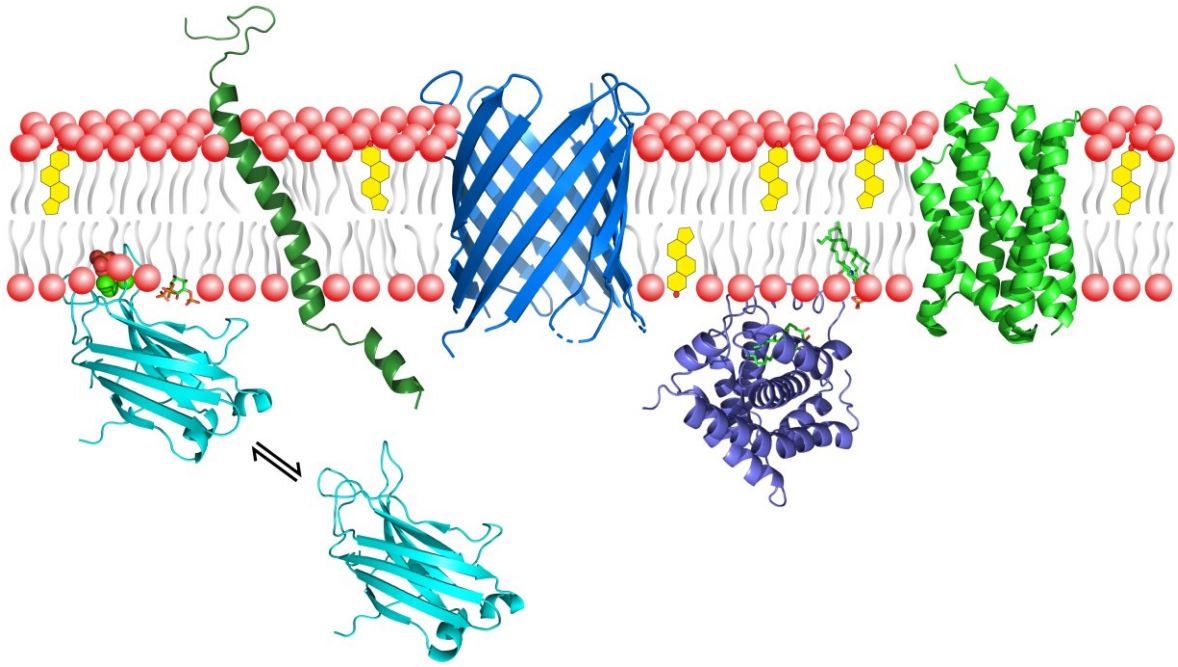

Fig. 3 Types of membrane proteins. Two groups of **peripheral**: one interacts reversibly upon biological stimuli (cyan), the other consists of proteins bound to the membrane via lipidic anchor (violet). **Integral membrane proteins**: span the thickness of membrane via a single (dark green) or multiple (light green) α-helices and β-sheet folded into a β-barrel (blue). Molecules of cholesterol are marked yellow. Structures of the proteins were adapted from the PDB database as follows: peripheral with reversible interaction (C2 domain with calcium binding activity): bound (3GPE)[16], unbound (3RDJ)[17]; peripherally attached via a lipid anchor (accelerated cell death 11 protein, 4NTI)[18]; integral: α-helices: single (insulin receptor transmembrane domain, 2MFR)[19] and multiple spanner (YetJ *Bacillus Subtilis* calcium channel)[20]; β-barrel (KdgM porin, 4FQE)[21].

Many human transmembrane enzymes and receptors span membranes with a single α-helical transmembrane domain (TMD)[22]. Generally, purification of such integral membrane proteins is problematic[23]. Thus, α-helical single spanning synthetic peptides with known amino acid sequence are used for membrane studies in simplified models[24–26]. They are good mimics of TMD and are much easier to work with then native proteins. In this thesis, transmembrane peptides with polyLeu sequence core were used. The polyLeu sequence forms a stable α-helix with high hydrophobicity[27], incorporates well into the model membranes[24,28] and these peptides were used in our laboratory prior to this work[24].

1.1.3 Biophysical properties of membranes

In previous paragraphs, components of biological membranes have been described, clearly implying the complexity of possible molecular interactions in these structures. These multiplex interactions influence membrane properties. Individual interactions contribute to

this effect with ranging intensity. These interactions are often closely related and selective influence of only one of those is usually impossible. Modifying a single parameter in cells may lead to changes in many membrane associated features and for that reason, biological membranes are often not suitable for studying their biophysical properties[29]. Unveiling the properties of membranes is the most readily done using simplified model systems, where the impact of particular membrane components can be specifically tested. Numerous model membrane systems have been developed to answer specific questions and enable the usage of diverse analytical method(s)[29]. In this thesis, large unilamellar vesicles (LUVs) were used as a model system.

One of the membrane properties which can be controlled by lipid composition, temperature and pressure is fluidity of membranes[30]. It is inherently connected to the mobility of molecules in the 2D plane of a membrane. Molecular mobility can be described by diffusion coefficient of membrane components[24,25]. Different lipid composition leads to diverse extent of mutual molecular interactions. Microscopic phase separation can be caused in some cases[31] with three main lipid phases distinguished. L_β phase (also known as solid phase S_o) with very restricted diffusion, forms membranes where hydrophobic tails are tightly packed. Liquid crystalline L_α phase (liquid disordered phase L_d) exhibits almost unhindered diffusion and high degree of freedom for rotation and movement of the molecules in the 2D plane of a membrane. Third phase is formed in the presence of cholesterol, called liquid crystalline ordered (L_o) phase. Its properties are intermediate to S_o and L_d[32]. Phase separation is caused by different transition temperatures of components in a membrane[31,33]. Microscopic visualisation of phase separation can be realised using lipids covalently labelled with fluorescent dyes or lipid-environment sensitive probes that preferentially incorporate to one of the phases[34]. Rate of the diffusion of membrane molecules can be also influenced by proteins. Recently, it was shown that even a single spanning transmembrane peptide can have a strong influence on the mobility of molecules in membranes. Roughness of the surface reduces molecular mobility of glycerophospholipids by reversible capturing of their acyl chains. At the same time, exclusion of cholesterol from the peptide's surface is observed. Such combined influence of cholesterol, that is known to reduce the glycerophospholipid mobility by membrane rigidification, and rough peptides leads to even a higher extent of reduction in membrane diffusion[24].

Membranes with different lipid composition often vary in their thickness. Length of fatty acyl chains, cholesterol and transmembrane proteins play an important role in membrane thickness changes[28,35]. Variation of membrane thickness in nanodomains containing cholesterol and sphingolipids was recently reviewed[32]. In case, that the length of TMD of the integral membrane protein and membrane thickness differs, hydrophobic mismatch occurs. The mismatch can be either positive where a TMD is longer than thickness of the membrane, or negative, when reversed. Integral membrane proteins can adapt to the hydrophobic mismatch in a number of ways, e.g. by clustering, tilting (only positive) or rearranging the position of flanking amino acids side chains as reviewed by Kilian in 2003[36]. Therefore, thickness can influence interactions between lipids and proteins in membranes.

Membranes containing oxidised phospholipids change their biophysical properties[37–39]. In case of fatty acyl truncation and addition of hydrophilic aldehyde or carboxy group at the chain break, the interaction between the interior of hydrophobic membrane and newly added polar group is no longer favourable. Both molecular dynamics (MD) simulations and solvent relaxation experiments with probes sensitive to membrane hydration show that oxidised acyls tend to orientate towards the membrane-water interface[37,39] leading to the voids formation at the acyl truncation spot[38]. Increased diffusion coefficient of lipids in membranes containing oxidised phospholipids has been also reported[39]. On the contrary, cholesterol decreases molecular mobility of oxidised lipids[40]. However, the impact of cholesterol on phospholipid diffusion with oxidised lipids is lower in comparison to the membranes with their absence[38]. MD simulation showed cholesterol insertion into void spaces in bilayer containing truncated phospholipids, suggesting its role in "healing" membranes containing truncated phospholipids[38].

1.2 Endoplasmic reticulum and unfolded protein response

Endoplasmic reticulum (ER) is the biggest organelle in eukaryotic cells. This membranous organelle is responsible for a storage of Ca^{2+}, protein and lipid synthesis or their homeostasis[41]. The ER-associated mRNA-ribosome complexes are responsible for the synthesis of all membrane and secreted proteins, but also for some cytosolic proteins[42]. A large scale proteosynthesis may lead to the accumulation of mis/unfolded proteins causing so-called ER stress. To achieve homeostasis, cells must adapt to the ER stress. Therefore, eukaryotic cells monitor folding capacity of ER by evolutionary conserved mechanism called the unfolded protein response (UPR)[41].

Upon the UPR activation there are three possible outcomes for a cell responding to the ER stress. Firstly, protein folding capacity can be restored by down-regulating translation and thus reducing the number of polypeptides entering the ER for folding. Second option is the ER expansion to increase the capacity of protein-folding machinery in a cell[43]. If above mentioned strategies for the homeostasis recovery fail, then a prolonged UPR activation can lead to more restrictive effects, including cell apoptosis[44].

1.2.1 UPR signalisation

Signal transducers recognise ER stress and initiate the UPR. Three signalisation branches are known[44]. Each branch recognises and reports on the ER stress differently, while sharing some features: e.g. a signal is transduced via a specific integral membrane protein in the ER. The most conserved UPR signal transducer is inositol requiring enzyme 1 (IRE1) which is the only UPR mechanism described in lower eukaryotes. Apart from IRE1, double-stranded RNA-activated protein kinase (PKR)–like ER kinase (PERK) and activating transcription factor 6 transduce UPR in mammals(ATF6)[45]. The depth of knowledge about the molecular mechanisms of signal transduction in each of these branches varies.

ATF6 contains large luminal, transmembrane and cytosolic N-terminal domains. Upon the accumulation of unfolded protein in the ER, ATF6 is packed into lipid vesicles and moved to the Golgi apparatus, where the luminal and cytosolic domains are cleaved off by site-1 and site-2 proteases[46,47]. Cytosolic (N-terminal) fragment [ATF6(N)] moves to the nucleus, where it triggers the expression of genes involved in the UPR, such as ER chaperone binding immunoglobulin protein[48]. Mechanism of ATF6 UPR signal transduction is depicted in **Fig. 4A** (p. 16).

PERK mechanism differs from that of ATF6. It forms dimers and gains a kinase activity leading to autophosphorylation followed by phosphorylation of translation initiation factor eIF2 α. The phosphorylation leads to inhibition of eIF2α activity and reduction of the amount of proteins entering the ER for folding. Low concentrations of unphosphorylated eIF2α lead to enhanced transcription of selected mRNAs, namely transcription factor ATF4, that induces the expression of another transcription factor C/EBP homologous protein (CHOP)[49]. CHOP mediates transcription of many genes and can lead to cell death by several pathways that have been recently reviewed[50]. One of the genes regulated by CHOP is growth arrest and DNA-damage inducible 34 gene (GADD34) that encodes an eIF2α phosphatase. In case of a brief activation of PERK, eIF2α phosphatase dephosphorylates eIF2α and mRNA

translation is regained (**Fig. 4B**)[48]. However, chronical activation of PERK branch leads to cell apoptosis[51]. PERK branch mechanism is depicted in **Fig. 4B**.

Third and the best understood branch of the UPR signal transduction from the ER is mediated by IRE1 protein (**Fig. 4C**). Activation of IRE1 begins with its clustering after the luminal domain of the protein recognises increased amount of unfolded proteins in the ER. Clustering induces autophosphorylation of IRE1 and formation of active RNase domain on the cytosolic side. X-box protein 1 (*XBP1*) precursor mRNA is then processed and translated into XBP1s protein that acts as a transcription factor inducing expression of chaperones, ER enzymes responsible for lipid biosynthesis and proteins of endoplasmic-reticulum-associated protein degradation (ERAD) pathway. IRE1's RNase domain also degrades mRNA, by which it decreases the amount of proteins entering the ER for folding[48].

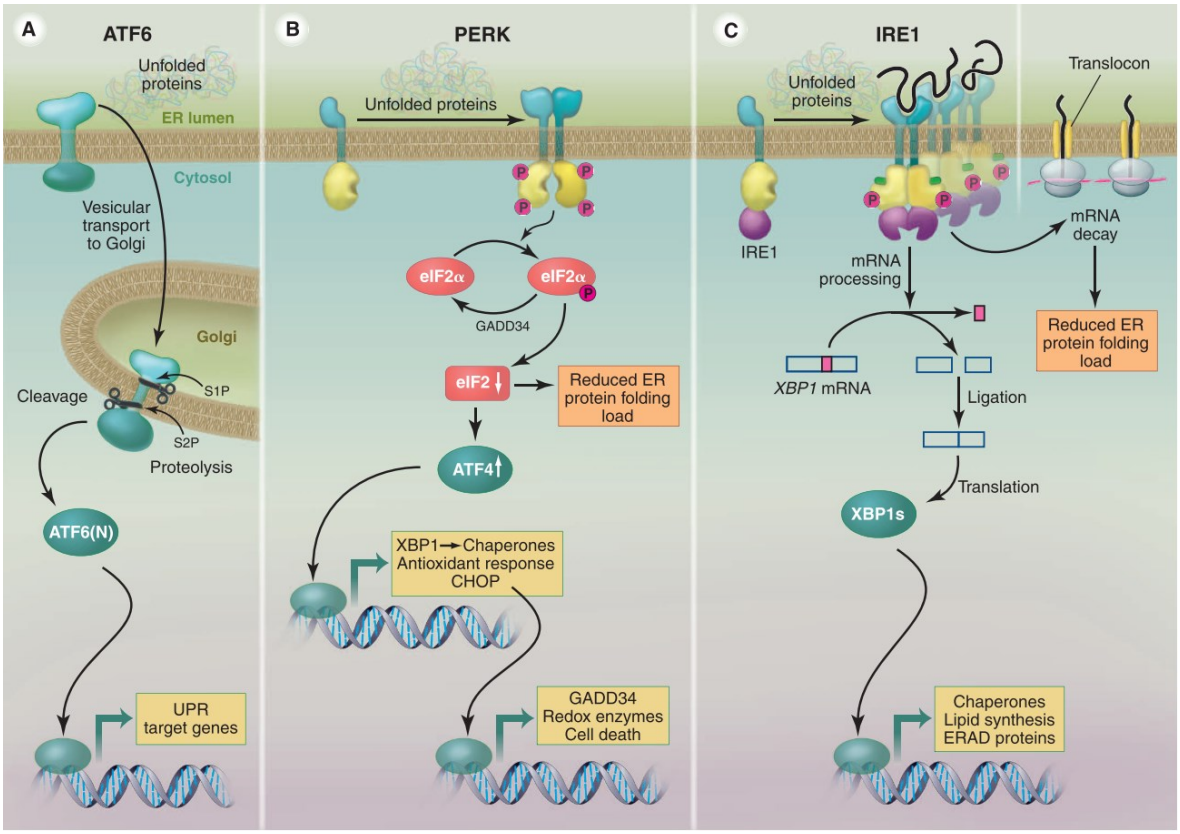

Fig. 4 Three branches of the UPR: Mechanisms of signal transduction by three ER membrane proteins (ATF6, PERK and IRE1). A: Upon recognition of unfolded proteins, ATF6 is moved to the Golgi apparatus in vesicles and cleaved. Its cytosolic domain then triggers transcription of chaperones. **B:** Recognition of unfolded proteins by PERK is followed by its dimerization, autophosphorylation and phosphorylation of eIF2α which leads to reduced protein translation. Consequent signalling can lead as far as cell apoptosis. **C:** Clustering of IRE1 upon recognition of unfolded proteins is associated with the protein autophosphorylation, formation of the active RNase domain, *XBP1* mRNA splicing and translation. XBP1s then regulates expression of chaperones, lipid biosynthetic enzymes end ERAD proteins. Figure was adapted[48].

1.2.2 UPR and lipid perturbation

So far, the UPR was discussed from the side of protein homeostasis response. IRE1 was first discovered in yeast[52] and connected to the inositol metabolism, therefore the name: inositol requiring 1 gene. Inositol is prerequisite and regulator of synthesis of phosphoinositol and its derivates[53]. Jonikas et al. showed strong UPR activation in yeast with deleted genes responsible for the regulation of lipid metabolism[54]. Further insight into lipid induced activation of the UPR via IRE1 was achieved by studies in the yeast cells that accumulated saturated fatty acids. Accumulation was achieved by extracellular feeding with saturated fatty acids or downregulation of the activity of Ole1p desaturase. Ole1p was downregulated by its complete deletion from genome (*ole1*Δ mutant) or Ole1p prosthetic group (haem) depletion in the cells lacking the δ-aminolevulinate synthase necessary for its synthesis. Accumulation by both feeding and Ole1p downregulation led to increased UPR activation[55]. In the same study, increased UPR activation was noticed in cells cultivated in medium containing ergosterol (the most prominent sterol in yeast). A noticeable reduction of UPR was achieved by the addition of unsaturated fatty acids or 4-phenyl butyrate (chemical protein chaperone) to the culture medium[55]. These results indicate the role of lipid saturation on UPR activation but do not demonstrate its contribution to any known mechanism of IRE1 signalling.

Steps to isolate the contribution of unfolded proteins and lipids to the activation of UPR led first to the mutation of IRE1 in the core stress-sensing region (CSSR) that is responsible for recognition of unfolded proteins in the ER lumen[56]. The ability of IRE1 with CSSR mutation to induce UPR upon inositol depletion was identical to the wild type protein. On the contrary, the mutant was insensitive to the cell treatment with tunicamycin or dithiotreitol that both cause disbalance in protein folding and induce the UPR by wild type IRE1[57]. Mammalian proteins IRE1α and PERK lacking luminal domain that recognises the unfolded protein presence in ER were able to form active clusters, suggesting that only transmembrane domain is required for the activation of UPR upon the perturbation of the cells with lipids (**Fig. 5**, p. 18)[58]. To clearly deny contribution of unfolded proteins, the effect of phospholipid acyl chain saturation on signal transducer PERK was also studied in isolated lipid vesicles. The addition of phospholipids with saturated fatty acyls to PERK-containing vesicles led to the aggregation of the protein[58]. Activation of the UPR signal transducers IRE1 and PERK by saturated lipids and cholesterol, thus seems to depend on specificity of transmembrane domain which recognises changes in membrane properties/composition.

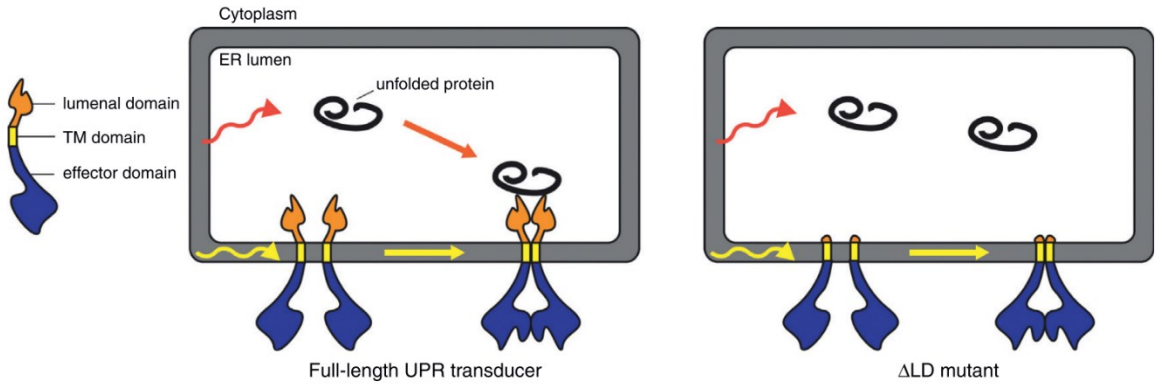

Fig. 5 Luminal domain is redundant for sensing lipid perturbations by UPR signal transducers in the ER. Unfolded protein related ER stress is depictured by orange curved arrow and lipid-induced stress by the yellow one. Figure was adapted[59].

Conservation of the TMD in UPR sensors has been investigated in the IRE1α that lacked the luminal – protein-sensing domain. Its TMD amino acid composition was scrambled or exchanged for the sequence corresponding to calnexin (different, unrelated ER membrane protein). In both cases, the mutant IRE1α remained responsive to the lipid-induced UPR[58]. Flow cytometry analysis of cells that encoded fluorescent proteins as reporters of the UPR further unveiled the mechanism that might be responsible for the UPR activation by IRE1α. The TMD sequence of IRE1α was mutated and exchanged for a non-specific α-helix of polyLeu by CRISPR/Cas9-mediated gene editing. IRE1α with exchanged TMD did not lose the ability to sense lipid perturbation in cells incapable of recognising unfolded proteins[60]. In yeast cells, IRE1 in which the native TMD was exchanged for polyLeu stretch, have been confirmed to properly incorporate into the ER membrane with similar reaction to the ER stress compared to the wild type by Halbleib et al. as well[61]. In their study they found an amphipathic helix adjacent to the TMD of IRE1 on luminal side of ER that was necessary for a proper function of IRE1[61]. In this study, Halbleib et al. performed also MD simulation where the insertion of amphipathic helix into the membrane resulted in membrane compression (**Fig. 6**, p. 19). Results of these MD simulations were used to postulate a molecular mechanism of the IRE1 clustering[61]. It states that IRE1 forms more stable aggregates in membranes that require more energy for compression, visualised as a hard spring in **Fig. 6** (p. 19), since the overall energy for membrane compression in aggregate of IRE1 is lower than in its monomeric form[61]. However, these results suggesting that the native amphipathic helix is required for IRE1 activation, could not be reproduced in mammalian cells with physiological levels of protein expression, by other group[60]. The discrepancy between these studies shows that a deeper insight into the topic is required. In both studies the ability of the IRE1 mutant with polyLeu TMD to form active clusters was shown[60,61]. In

this thesis, clustering mechanism of polyLeu helices was studied in synthetic bilayers with different lipid composition.

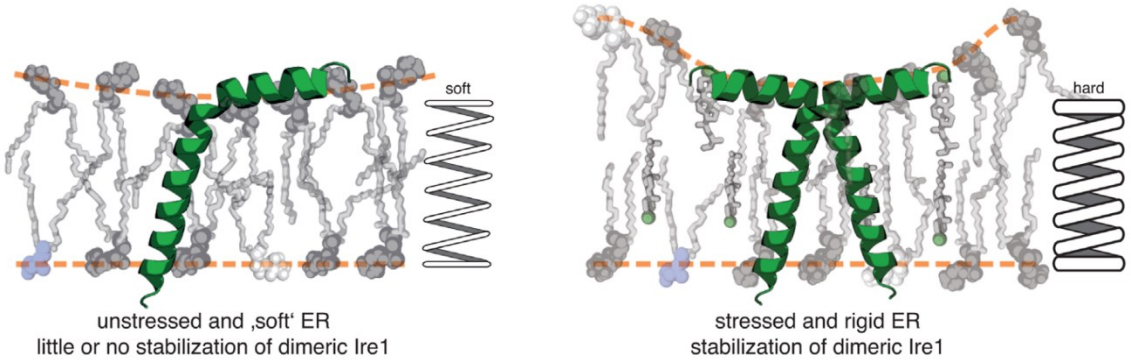

Fig. 6 A proposed mechanism of IRE1 clustering in rigidified membranes. Left: IRE1 monomer does not require stabilisation when ER membrane is unstressed ("soft") and the compression of such a membrane does not require high energy. Right: In the ER membrane undergoing stress response, lipids contributing to the membrane rigidity are present. In such conditions, IRE1 is stabilised by aggregation, because the energetic cost for membrane compression in this system is higher. Figure was adapted[62].

1.2.3 Other sensor of membrane properties

In addition to IRE1, other proteins are capable of sensing the alterations in lipid composition of membranes. Mga2 is a protein located in the membrane of ER and controls the expression of Ole1 desaturase[63]. It is a single membrane spanning protein, that can form more stable homo-dimers in tightly packed membranes[64]. The TMD of Mga2 rotates freely in the membrane. In more rigid membranes, a higher population of conformers capable of transcription factor activation is present (**Fig. 7**)[64].

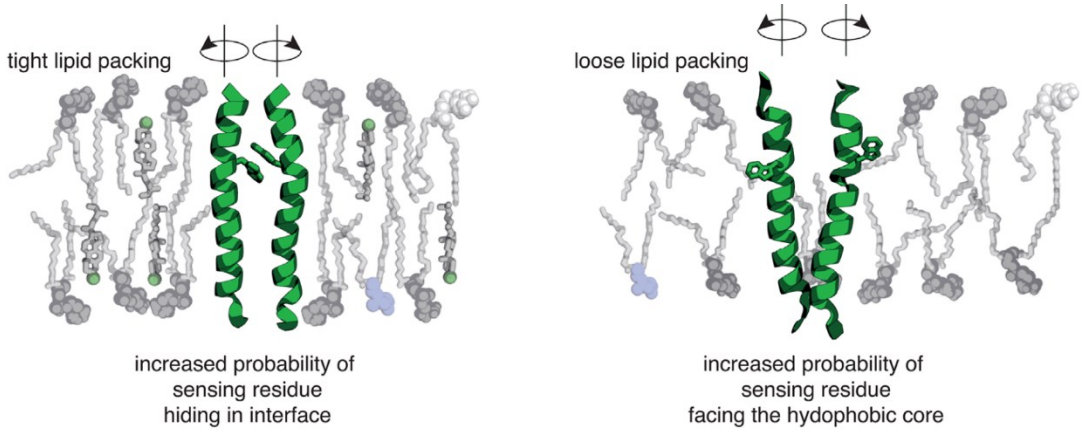

Fig. 7 A proposed mechanism of lipid packing sensing by Mga2. TMD of Mga2 rotates under tested membrane conditions. A higher population of activating homodimers was present in membranes with tight lipid packing. Figure was adapted[62].

Biological membranes composed mainly of lipids and proteins are extremely variable. Their properties and composition are changing rapidly in order to ensure cell and organelle

homeostasis. The ER is the largest organelle in eukaryotic cells. To maintain physiological properties of these membranous structures, sensors of pathological processes have developed. For a proper function of the ER, its membrane must remain highly fluid. Recent studies indicate that ER membrane proteins known to induce UPR upon ER stress recognition (IRE1, PERK), might also function as sensors of lipid packing in this organelle. The molecular mechanism of lipid-induced activation of these proteins remains elusive as contradictory results have been published. This thesis aims to shed a light on a possibility that changing membrane properties can induce clustering of transmembrane peptides irrespective of their amino acid sequence.

2 Aims and objectives

This work aims to study whether lipid composition of model membranes (liposomes) induces clustering of model transmembrane peptides LW21A and LW21B. Question arises from the research of single spanning receptors which are capable of sensing lipid perturbation in the ER of living cells. The work includes these individual tasks:

- preparation of liposomes with different lipid composition
- quality control of formed liposomes by dynamic light scattering
- measurement of time resolved anisotropy decays of Trp fluorescence
- comparison of anisotropy decays to determine the level of peptide clustering
- automatization of the data analysis

3 Material

3.1 Instruments

- IBH 5000U Time Resolved Spectrofluorimeter – Horiba, Japan
- Zetasizer Nano S – Malvern Instruments, UK

3.2 Chemicals

- 1,2-dioleyl-sn-glycero-3-phosphocholine – Avanti Polar Lipids, USA
- 1,2-dinervonyl-sn-glycero-3-phosphocholine – Avanti Polar Lipids, USA
- 1,2-dipalmitoyl-sn-glycero-3-phosphocholine – Avanti Polar Lipids, USA
- 1-palmitoyl-2-glutaryl-sn-glycero-3-phosphocholine – Avanti Polar Lipids, USA
- 1-palmitoyl-2-oleoyl-glycero-3-phosphocholine – Avanti Polar Lipids, USA
- 2,2,2-trifluoroethanol – Alfa Aesar, USA
- chloroform – VWR Chemicals, USA
- cholesterol – Avanti Polar Lipids, USA
- glucose – Sigma Aldrich, USA
- HEPES – Sigma Aldrich, USA
- L-tryptophan – Sigma Aldrich, USA
- methanol – Honeywell Riedel-de Haën, Germany
- miliQ water – Milipore, USA
- NaCl – Sigma Aldrich, USA
- palmitic acid – Sigma Aldrich, USA
- synthetic peptide Cys-LW21 – Biomatik, Canada
- synthetic peptide LW21A – Vidia, Czech Republic
- synthetic peptide LW21B – B-Cube, Germany

3.3 Other equipment and material

- Disposable UV-Micro Cuvettes – Brand GmbH & Co KG, Germany
- Extruder LiposoFast-Basic – Avestin, Canada
- LUDOX HS-40 Colloidal Silica Beads – Sigma Aldrich, USA
- Nucleopore Track-Etched Membranes, 100 nm pore size – Whatman, UK
- QS Ultra-Micro Quartz Cuvette, 3mm – Hellma Analytics, Germany

4 Methods

4.1 Verification of used peptides by mass spectrometry

In order to maintain maximum control over the model system used in this thesis, molecular mass of the used peptides was analysed by mass spectrometry. 50 µg of lyophilised peptide was dissolved in 500 µl of trifluoroethanol (TFE), then further diluted in mixture of acetonitrile and water (ACN:H_2O, 1:2 vol%) to a final concentration of 1 ng/µl. The peptide solution was directly injected and analysed by mass spectrometer. Positive electrospray ionisation with ion synchrotron resonance detection (SolariX, Bruker) was used. Measurement and analysis were performed by Zdeněk Kukačka.

4.2 Preparation of model membranes

Lipid composition of biological membranes is complex. This allows for a quick adjustment in membrane composition of the living cells for rapid recovery of homeostasis[65]. Therefore diverse model membrane systems are used for comprehensive studies of lipid dependent changes in membrane properties[29]. In this thesis, liposomes in the form of LUVs were used as a model membrane system. Possible molecular mechanisms of transmembrane protein (peptide) cluster formation was probed by the adjustment of their lipidic composition.

Liposomes were prepared as follows. First, 50 µM solution of peptides in TFE was prepared. Organic solutions of lipids and peptides were then mixed in tube to reach desired composition. Lipid film was prepared by the evaporation of organic solvents under nitrogen at ambient temperature. Lipid films were further dried under vacuum for at least 30 min to remove residual organic solvents. Lipid film was hydrated with 300 µl of 105 mOsm HEPES buffer (>60 mM glucose; 10 mM HEPES; 10 mM NaCl; pH 7,4; filtered – pore size 0,22 µm) to form a multilamellar vesicles (MLVs). Concentration of all membrane components in MLVs was 0,5 mM. Lipid films containing DPPC were hydrated in a buffer pre-heated to approximately 60°C, i.e. above the gel transition temperature of DPPC (41°C)[66]. After a short incubation in the buffer, lipid films were agitated repeatedly on vortex mixer until no film was visible at the bottom of the test tubes. MLVs were then transferred to Hamilton syringe and downsized by repeated extrusion (21-times) through polycarbonate membranes with pores of defined diameter (100 nm). Liposomes containing DPPC were downsized in the extruder placed inside the holder that was heated to 60°C. Hamilton syringes and extruder were cleaned by sonication in dH_2O, rinsed in MeOH and miliQ water prior to use. In **Fig. 8** (p. 24) is depicted the process of liposome preparation.

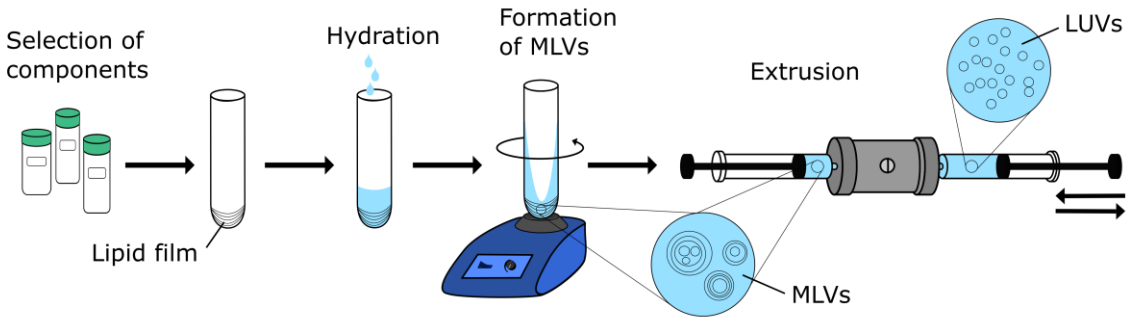

Fig. 8 Liposome preparation process. First, components of model membrane are selected, pipetted into a tube and dried to remove residual organic solvents, leading to the formation of a visible lipid film. The film is hydrated in the next step. Vigorous agitation of a hydrated lipid film using vortex mixer forms MLVs. One of the possible ways to downsize MLVs is their extrusion through polycarbonate membrane with defined pore diameter. This leads to the formation of LUVs.

Liposomes were prepared in batches. Each batch contained model membranes with a specific lipid composition described for each experiment and controls with constant composition of lipids and peptides. As the primary control, liposomes containing only DOPC were prepared. This composition was used to assure the proper formation of vesicles and determine maximum possible concentration of vesicles formed with a given preparation method. The thesis focuses on studying clustering of peptides and proper control samples for aggregated and non-aggregated peptides were needed. For monomeric control sample, liposomes with 3 mol% of LW21A in DOPC were used. Monomeric state of LW21A peptides in this composition was confirmed in our laboratory prior to this work[24]. As a control of a dimeric state, liposomes containing 3 mol% of Cys-LW21 peptide in DOPC were used. Cys-LW21 contains terminal cysteines that can form disulphide bridge when oxidised. Dimeric state of this composition was confirmed in our laboratory prior to this work[24]. Amino acid sequences of all used peptides are in **Tab. 1**.

Tab. 1 Amino acid sequences and the predefined state of used peptides in control vesicles containing DOPC. In sequences, positively charged residues are highlighted in blue, negatively in red, N-terminal cysteine responsible for dimerization is underlined, tryptophan is in bold and α-helical TMD is boxed.

Name	Amino acid sequence	State*
LW21A	GLLDSKK**WW**LLLLLLLLALLLLLLL**WW**KKFSRS-amid	M
LW21B	SGGSDK**WW**LLLLLLLLALLLLLLL**WW**KDSGGS-amid	n.d.
Cys-LW21	CGGLLDPKK**WW**LLLLLLLLALLLLLLL**WW**KKFSRS-amid	D

* *State of peptide is considered in only DOPC containing model membrane*[24]*. M stands for a monomeric and D for a dimeric state. State of LW21B was not determined prior to this work.*

To test different membrane environment conditions, liposomes containing cholesterol, palmitic acid (PA), phosphatidylcholines containing saturated, unsaturated and oxidised fatty acids with different alkyl length were prepared. Alteration of lipidic composition led to changes in membrane properties of model systems as defined in a numerous previous works reviewed in Cebecauer et al., 2018[32]. The molar composition of prepared vesicular components is in **Tab. 2**.

The available amount of the original LW21A peptide used in Olšinová et al, 2018[24] was only sufficient for three tests with varying lipid compositions (**Tab. 2**). Because of that the rest of the experiments were performed using the updated version of LW21A which we call LW21B and it has a slightly altered amino acid sequence (**Tab. 1**, p. 24). The changes made in the sequence were based on our previous experience from working with the original LW21A and included substitution of one Lys to Asp on both sides of the hydrophobic part. This was introduced to decrease the electrostatic repulsion between peptides. Both ends of the peptide were adapted to mirror each other (**Tab. 1**, p. 24). The original LW21A peptide contained flanking residues adapted from the TMD of TCRζ-chain[67]. These are naturally adjusted for the insertion into an asymmetric membrane. Formation of asymmetric model membranes is not yet established in our laboratory. Thus, we designed symmetric terminal sequences in the newly designed peptide LW21B.

Tab. 2 Composition of prepared liposomes. Molar percentage of lipids and peptides in all prepared vesicles. Each row represents one lipid composition. LW21A, LW21B and Cys-LW21 are peptides.

DOPC	POPC	DPPC	PGPC	24:1PC	CHOL	PA	LW21A	LW21B	Cys-LW21
100									
97							3		
97								3	
97									3
87						10	3		
87						10		3	
87			10					3	
72					25		3		
72					25			3	
62			10		25			3	
47	50							3	
	97							3	
	87		10					3	
	72				25			3	
	62		10		25			3	
		72			25			3	
				97				3	

4.3 Verification of liposome formation by dynamic light scattering

After liposomes preparation, each batch was analysed by dynamic light scattering (DLS). DLS is a method also known as quasi-elastic light scattering or photon correlation spectroscopy. Particles in solution scatter incident laser light which is measured on the detector. Signal fluctuation is then recorded and autocorrelated. By fitting the autocorrelation function, information about the diffusion of particles in solution can be gained. Size distribution of dissolved particles is connected to the diffusion coefficient. It is inversely proportional to the diameter of spherical particles in solution[68]. Thus, this method is used to determine distribution of liposome diameters after downsizing of MLVs by extrusion. Additional information about the concentration of prepared liposomes is extracted from measured count rate. A simplified scheme of a DLS measurement is depicted in **Fig. 9**.

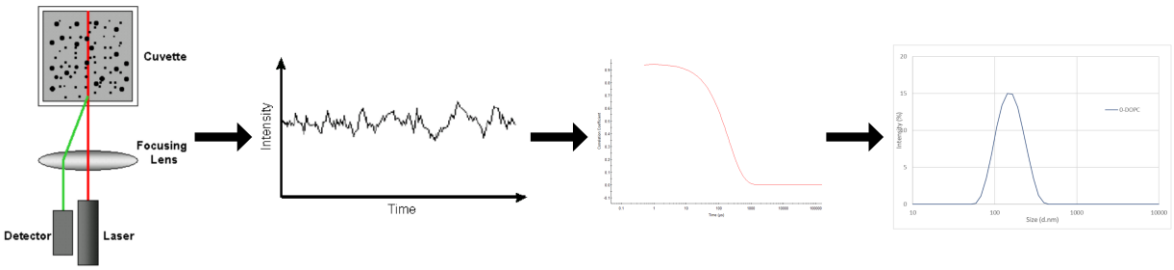

Fig. 9 Basic principle of DLS. Time fluctuation of light scattered from a sample is measured. Autocorrelation function of fluctuating signal is computed and fitted, giving rise to size distribution of particles in solution. Figure was adapted and adjusted[69].

Zetasizer Nano S (Malvern Instruments, UK) was used for quality control of formed vesicles by DLS. Measurement parameters, laser intensity and position of data acquisition (measurement depth) were adjusted automatically by the instrument, which was pre-set for the measurement of liposome sizes in water solution at room temperature. Disposable cuvettes for small volumes of sample were used. Measurements for each lipidic composition were repeated three times. Parameters of measured curves were acquired immediately after measurements from Zetasizer software. Size distribution curves were exported and plotted in Excel using the macro, that automatically averages triplicate measurements and plots all measured points with standard deviation. Macro was written as a part of diploma thesis and the code is attached on the CD at the end of thesis (for details see **Tab. 3**, p. 31).

4.4 Fluorescent properties of tryptophan

Methods of fluorescence spectroscopy were used for study of transmembrane peptides in this thesis. Because of that, general spectral properties of tryptophan (Trp) and brief

information about Förster Resonance Energy Transfer (FRET) will be discussed in this section.

Trp is the aromatic amino acid that contributes to the protein absorbance at 280 nm to the greatest extent[2]. After excitation, molecules of Trp emit fluorescence with the emission maxima at 330-350 nm depending on their microenvironment[70]. These properties can be used to study proteins containing Trp by spectroscopic methods without a need to label the molecules with additional chromophores[71]. Transmembrane model peptides used in this study contain four Trp residues at the water-bilayer interface (two at each side, see **Tab. 1,** p. 24).

The overlap between the excitation and emission fluorescence spectra of any fluorescent dye can lead to phenomenon called FRET. This applies also to fluorophores of the same kind. The dye responsible for light absorption is referred to as donor and the one excited resonantly is acceptor. The process is accelerated when the dyes are appropriately oriented and located in close vicinity. Generally, the optimal distance between fluorophores to successfully transfer energy by FRET lies between 1 to 10 nm[72]. If the energy is transferred between the same molecules, it is referred to as homo-FRET. Due to the existence of homo-FRET, the fluorescence properties of Trp can be used to learn about the average mutual distances of Trp-containing peptides (e.g. LW21) embedded in the membrane[24]. Since the same kind of fluorophores is used, a change in spectral properties of Trp fluorescence by homo-FRET cannot be directly observed. To overcome this obstacle, confirmation of the close vicinity of the two Trp in peptides is determined by the changes in time resolved fluorescence anisotropy[72].

4.5 Time corelated single photon counting

In order to gain information about the homo-FRET occurrence by time resolved fluorescence anisotropy, time resolved decays of Trp fluorescence are determined. For this purpose, time corelated single photon counting (TCSPC) is employed. This method requires pulsed excitation and single photon detectors to measure arrival times of photons emitted after the excitation. The result of such measurement is a histogram of photon arrival times (decay of fluorescence). Fitting the measured decay with the proper mathematical model leads to the information about the fluorescence lifetime(s) of a fluorophore under the applied experimental conditions[73]. Principle of TCSPC is depicted in **Fig. 10**, (p. 28).

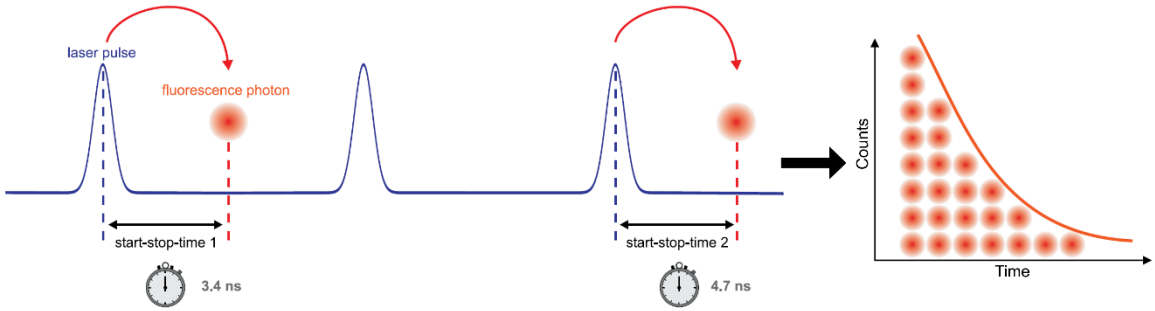

Fig. 10 Principle of TCSPC. Repeated measurement of time difference between laser excitation pulse and photon arrival generates a histogram of photons with specific times of arrival. Figure was adapted and adjusted[73].

4.6 Time resolved fluorescent anisotropy measurement

What is behind the fact that the anisotropy is altered when homo-FRET occurs? When exciting fluorophores with polarised light, a biased excitation occurs. Preferentially dyes with the absorption transition vectors aligned parallel to the polarisation plane of the light are excited. This phenomenon is called photoselection. The orientation of emitted fluorescent light is well defined shortly after the excitation. With time, it becomes more random[74]. Sources of randomization are for example rotation of molecules or the effect of homo-FRET. In the theoretical case, where free dyes in solution have parallel absorption and emission transition vectors, homo-FRET process is not occurring. Then, only the rotation of molecules contributes to the anisotropy decay. In this case anisotropy curve describes the kinetics of molecular rotation. When homo-FRET is involved, the energy from donor is transferred to acceptor which is oriented differently. In this case, the emission light is depolarized faster (than in the absence of homo-FRET). The phenomenon can be detected as a faster drop of the anisotropy curve[72]. The principle of the homo-FRET effects on time resolved anisotropy is depicted in **Fig. 11**.

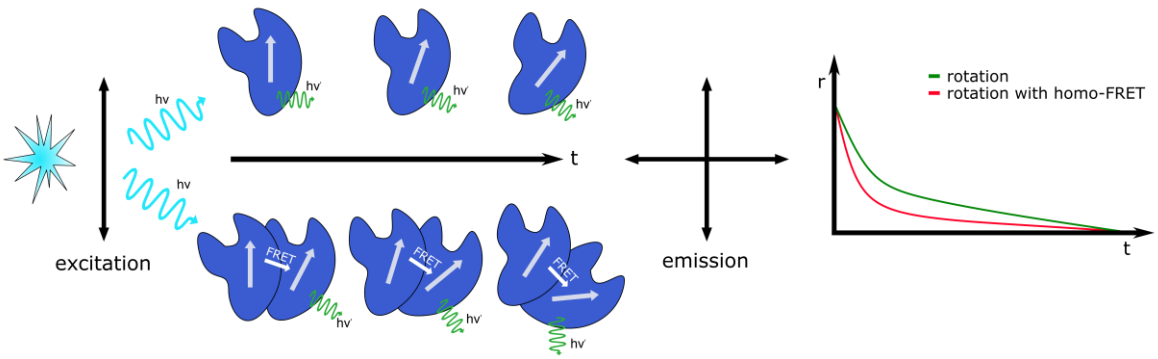

Fig. 11 Principle of time resolved anisotropy. Chromophores are excited by polarized light. Two time resolved emission decays are measured with different orientation of emission polarizers. The decay of anisotropy with rotational emission depolarization only is different to the one determined for the combined effect of rotation and homo-FRET process.

Interpretation of time resolved anisotropy decays can be complex. In some cases, it is possible to address changes in a studied system by simple comparison of decay curves (**Fig. 11**, p. 28)[75]. Decays of anisotropy cannot be usually measured directly. Two time resolved fluorescent decays must be determined with different orientations of the emission polarizers. The first measurement is performed with the emission polariser oriented vertically (VV) and the other one with the polarizer in the horizontal position (VH). The first letter in the labels corresponds to constant vertical orientation of the excitation polarizer. The second letter indicates vertical (V) or horizontal (H) orientation of the emission polarizer. Anisotropy decay curve is calculated by applying the following mathematical formula onto measured VV and VH decays:

$$r(t) = \frac{VV(t) - G.VH(t)}{VV(t) + 2.G.VH(t)} \quad (1)$$

where *r* is anisotropy, *VV* and *VH* are fluorescence intensities (counts) at time *t*, with emission polariser rotated to vertical and horizontal position, parallel and perpendicular to the excitation polariser, respectively, and *G* is the factor correcting for the different detection efficiency of the vertically and horizontally polarised fluorescence (see below for G-factor description)[74].

Measurements were performed on IBH 5000U Time Resolved Spectrofluorimeter (Horiba, Japan). Prior to each measurement, optimal conditions for Trp fluorescence measurement were assured using 50 μM Trp solution in 105mOsm HEPES buffer (see liposome preparation section for details) to get a maximum signal on the detector. In the first step, XY position of cuvette was adjusted to the centre of light path. Then position of lens along both excitation and emission light path was adjusted. Subsequently, scattering from the Ludox colloidal silica beads was utilized to determine the optimal position of both excitation and emission polarisers, i.e. the maximum signal from the scattering solution corresponded to the vertical-vertical position of the polarizers When the proper position of the cuvette and polarisers was set, TCSPC measurements of Trp fluorescence in peptides were performed.

Trp in LW21 peptides were excited by 295 nm pulsed UV diode at 5 MHz repetition rate (PicoQuant, Germany). Emission monochromator was set to 350±16 nm (32 nm spectral bandwidth) and photons were detected on multichannel plate photomultiplier. Grid polarizers were inserted to both excitation and emission light path to ensures passage of light

with desired plane of oscillation. Excitation polarizer was always oriented vertically. The emission polarizer was repeatedly rotated from vertical to horizontal position after 60 s long acquisition of VH or VV decay. Measurement was finished when the difference between the VV and VH maxima of the fluorescence decays reached 50 000 counts. TCSPC card was set to 2048 time channels, leading to the width of a single channel (time resolution) equal to 57,25 ps. Such temporal resolution guaranteed reasonable measurement times for Trp whose fluorescence is relatively weak (ε_{280} = 5600 $cm^{-1}.M^{-1}$) compared to regularly used organic fluorescent dyes such as Rhodamine 6G (ε_{530} = 116 000 $cm^{-1}.M^{-1}$)[76,77].

4.7 Data analysis of fluorescent decays

For the analysis of anisotropy, vertical and horizontal fluorescence decays were processed using the FluoFit software (PicoQuant, Germany). At first, G-factor that describes the different sensitivity of the set-up to the vertically and horizontally polarised fluorescence, was calculated by a tail fit of decays measured in 50 μM solution of free Trp in 10 mM HEPES buffer with >60 mM glucose (105 mOsm). Using the acquired G-factor, time resolved anisotropy decays were calculated. These decays were then exported and compared using Excel spreadsheet software (Microsoft, USA).

4.8 Automatization of data comparison

Software for fast and easy comparison of measured time resolved anisotropy curves is not available and manual loading of data into Excel is time consuming. So, I have decided to automatize this process. Macro for Excel was written in VBA (Visual Basic for Applications, Microsoft, USA) to complete the comparison of time resolved anisotropy curves.

Whole automatization process was divided into several steps in order to control successful completion of each one. The other reason for sub-organisation of macro was to make each macro shorter and easier to revise when troubleshooting.

In the first part, data import was optimised. In the next step, data were read and plotted into the graph. Other macros were created for summarising the fit parameters and manual alignment of the curves for the more precise overlap of the beginning of anisotropy decay curves (**Tab. 3**, p. 31). All the code is attached on CD at the end of the thesis in both .txt and .xlsm (Excel sheet with macros) formats.

Tab. 3 Excel macros written for the purpose of this thesis in VBA. All codes are available on the attached CD at the back-cover of the thesis. Codes are filed in both .xlsm and .txt formats.

Name	Function of macro	Sub-organisation
DLS size plot	Plotting the size distribution of LUVs from DLS measurements	Import and reading of data Averaging data from repeated measurements Plotting the curves
Anisotropy plot	Comparison of time resolved decays of anisotropy	Import of files from FluoFit Reading the imported files Plotting the measured curves Copying parameters to new excel file Shift of decay beginning if needed

5 Results

5.1 Sample preparation and verification

Liposomes in form of LUVs were used as a model membrane system in this study. They were prepared by repeated extrusion and their size distribution was verified by DLS. Due to the practical aspects concerning the time required for preparation of LUVs and measurement of time resolved anisotropy, model membranes were prepared in batches containing 5-6 different compositions of liposomes.

5.1.1 DLS analysis of LUVs containing LW21A and LW21B peptide

Fig. 12 (p. 33) compares size distribution of LUVs with a simple lipidic composition. DOPC is the only lipid present in these vesicles. In grey, size distribution of control liposomes lacking the peptide is plotted. Red and blue curves correspond to vesicles containing DOPC with 3 mol% of LW21A and LW21B, respectively. Mean hydrodynamic diameter is slightly higher than the pore size of membranes used for extrusion (100 nm), as generally reported[78]. Decrease of diameter of liposomes containing LW21A peptide compared to DOPC only is noticeable (see column Peak Mean in **Tab. 4**, p. 33). The potential explanation is the difference in bilayer elasticity between liposomes without and with the peptides. Liposomes that are capable of higher degree of deformation prior to disintegration will pass the pores and regain the spherical shape after the pore passage. Therefore, the higher hydrodynamic radius of only DOPC vesicles. Percentual area of plotted peak in all composition present is 100 %, confirming successful downsizing of MLVs and formation of vesicles with a desired size. Polydispersity index describes width of measured distribution (PdI in **Tab. 4**, p. 33). It is higher for peptide-containing vesicles. Derived count rate of scattered light can be used for comparison of liposomal concentration within one measurement. The concentration of DOPC containing vesicles is ~3-times higher compared to those containing transmembrane peptides. This implies that the presence of peptide in the MLVs decreases the amount of formed of LUVs.

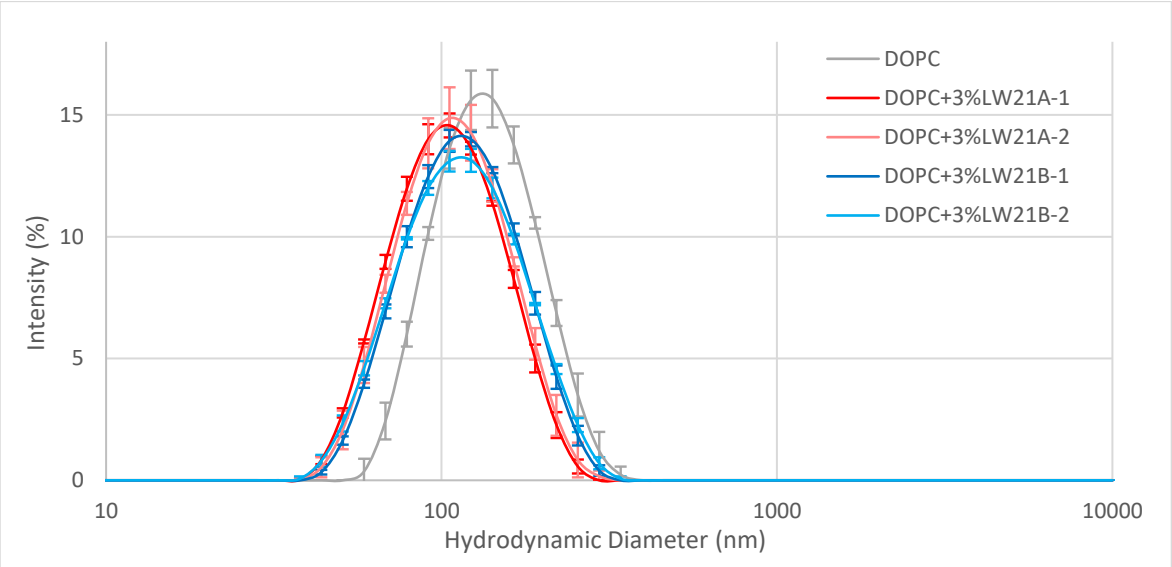

Fig. 12 Size distribution of DOPC liposomes containing LW21A or LW21B peptide measured by DLS. DOPC is the only lipidic moiety present. Control liposomes are plotted in grey. The peptide-containing vesicles with 3 mol% LW21A or LW21B are plotted in red or blue, respectively.

Tab. 4 Quantitative analysis of DLS measurements performed on liposomes containing DOPC with LW21A or LW21B peptide. All parameters were gained/calculated automatically using Zetasizer software from three measurements. Size distribution of the vesicles is plotted in **Fig. 12.**

Vesicular Composition	Peak Mean (d. nm)	Peak Area (%)	PdI	Derived Count Rate (kcps)
DOPC	142,7	100	0,096	6,85E+04
DOPC+3%LW21A-1	111,2	100	0,116	2,31E+04
DOPC+3%LW21A-2	115,2	100	0,125	2,25E+04
DOPC+3%LW21B-1	123,1	100	0,154	2,64E+04
DOPC+3%LW21B-2	123,1	100	0,162	2,69E+04

5.1.2 DLS analysis of LUVs containing cholesterol and PA

Model membranes containing DOPC as a main lipidic component with the addition of cholesterol or palmitic acid (PA) were also prepared with LW21A or LW21B peptide.

Size distribution of liposomes with LW21A is depicted in **Fig. 13** (p. 34). Distribution of control LUVs with DOPC only is plotted in grey and vesicles containing DOPC with 3 mol% of LW21A in red. Change in membrane properties was accomplished by the addition of 25 mol% of cholesterol or 10 mol% of PA. Their distributions are plotted in blue and green, respectively. **Tab. 5** (p. 34) contains quantitative parameters calculated during DLS measurements of size distribution plots depicted in **Fig. 13** (p. 34). Both plots and parameters show slightly bigger vesicles than membrane pore size that was used for the extrusion (100 nm). LUVs containing peptide combined with more complex lipidic composition

resulted in smaller hydrodynamic diameter compared to LUVs with DOPC only. Model membranes with PA (green curve) display also particles with hydrodynamic diameter in micrometre region. Presumably, this was caused by sample contamination with dust particles that accidentally entered the solution of prepared LUVs. The broadest distribution of sizes is present in the composition with PA which is reflected also in the highest PdI value (see **Tab. 5**). Derived count rate indicates similar concentration of proteo-liposomes containing DOPC and DOPC with 25 mol% cholesterol while LUVs containing PA displayed a lower count rate. Scattered signal measured for the control liposomes containing DOPC only is again ~3-times higher compared to the rest of prepared liposomes (see **Tab. 5**, p. 34).

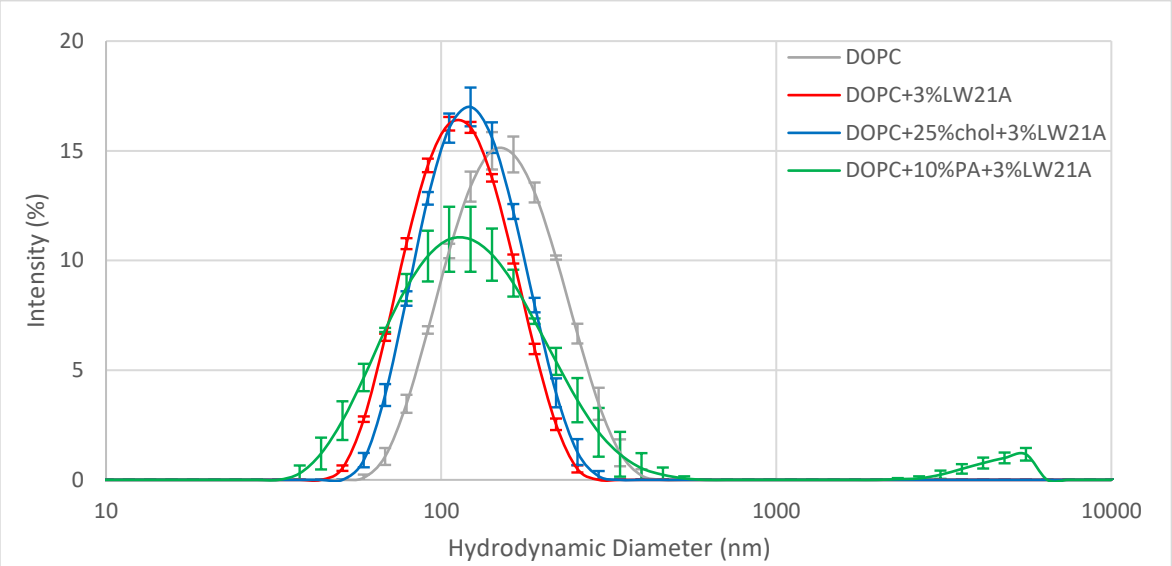

Fig. 13 Size distribution of liposomes with LW21A in presence of DOPC and cholesterol or PA measured by DLS. Formation of control LUVs containing DOPC are plotted in grey, liposomes with DOPC and 3 mol% of LW21A in red. Vesicles composed of DOPC, 3 mol% of LW21A and 25 mol% of cholesterol or 10 mol% of PA are plotted in blue or green, respectively.

Tab. 5 Quantitative analysis of DLS measurements performed on liposomes containing cholesterol or PA in addition to DOPC and LW21A peptide. All parameters were gained/calculated automatically using Zetasizer software from three measurements. Size distribution of the vesicles is plotted in **Fig. 13**.

Vesicular Composition	Peak Mean (d. nm)	Peak Area (%)	PdI	Derived Count Rate (kcps)
DOPC	162,5	100	0,120	5,81E+04
DOPC+3%LW21A	118,9	100	0,091	2,16E+04
DOPC+25%chol+3%LW21A	128,8	100	0,090	2,36E+04
DOPC+10%PA+3%LW21A	133,9	96,3	0,253	1,34E+04

Preparation of LUVs containing the same lipidic species as those in **Fig. 13** and **Tab. 5** was repeated also in the presence of LW21B peptide. The size distribution curves of this

batch are plotted in **Fig. 14** with curve parameters in **Tab. 6**. Mean hydrodynamic diameter increases for LUV batch with LW21B peptide in the following order: peptide, DOPC and PA; peptide with DOPC; peptide, DOPC and cholesterol to peptide free, control with DOPC only (**Tab. 6**). LUVs with DOPC and peptide (red curve in **Fig. 14**) displays particles with mean distribution around 25 nm. Width of the size distribution is the lowest for DOPC control vesicles and increases for peptide containing LUVs in order: PA, cholesterol to DOPC only. Concentration of formed LUVs with peptide is again ~2-3-times lower than that of DOPC control (see Derived Count Rate in **Tab. 6**)

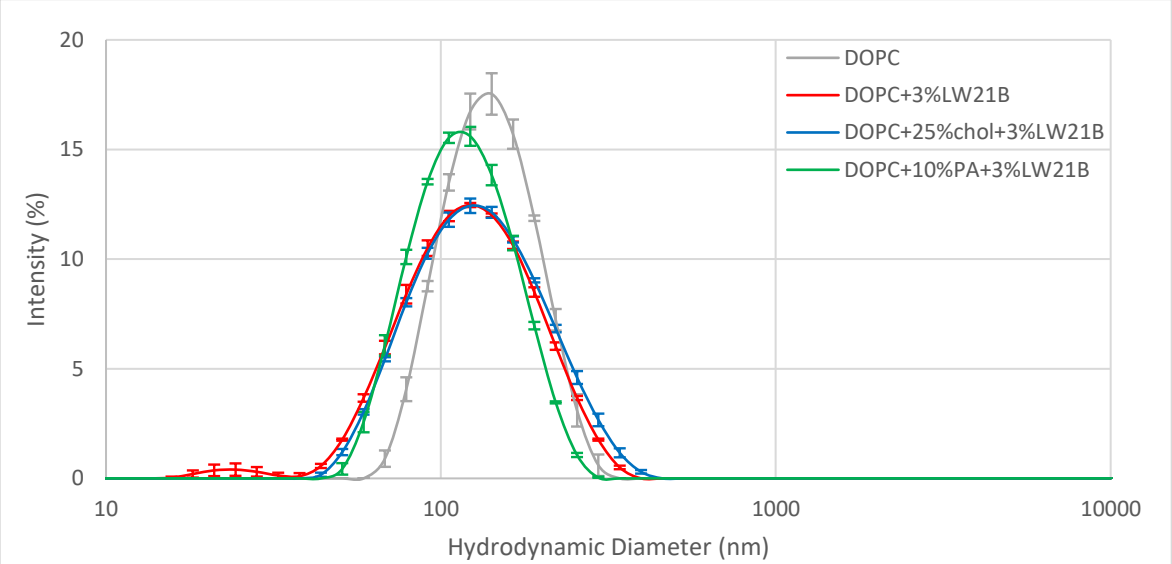

Fig. 14 Size distribution of liposomes with LW21B in presence of DOPC and cholesterol or PA measured by DLS. Formation of control LUVs containing DOPC are plotted in grey, liposomes with DOPC and 3 mol% of LW21B in red. Vesicles composed of DOPC, 3 mol% of LW21B and 25 mol% of cholesterol or 10 mol% of PA are plotted in blue or green, respectively).

Tab. 6 Quantitative analysis of DLS measurements performed on liposomes containing cholesterol and palmitic acid with LW21B peptide. All parameters were gained/calculated automatically using Zetasizer software from three measurements. Size distribution of the vesicles is plotted in **Fig. 14**.

Vesicular Composition	Peak Mean (d. nm)	Peak Area (%)	PdI	Derived Count Rate (kcps)
DOPC	145,4	100	0,079	6,02E+04
DOPC+3%LW21B	133,7	98,5	0,186	2,02E+04
DOPC+25%chol+3%LW21B	141,7	100	0,154	2,51E+04
DOPC+10%PA+3%LW21B	122,7	100	0,102	2,88E+04

5.1.3 DLS analysis of LUVs with increased fatty acyl chain saturation

Batch of LUVs with different level of fatty acyl saturation was prepared only in the presence of LW21B.

Size distributions of LUVs in this batch are plotted in **Fig. 15**. Liposomes contained 3 mol% of LW21B, except for LUVs control with DOPC only (grey). Lipid composition of remaining LUVs in this batch was: reference composition with DOPC (red); DOPC and 50% POPC (dark blue); POPC only (light blue); POPC and 25 mol% cholesterol (dark green); DPPC and 25 mol% of cholesterol (light green). As shown previously, liposomes formed by extrusion are bigger than the pores used for the extrusion. The largest mean hydrodynamic diameter was measured for control LUVs (grey) and the smallest for vesicles containing only one lipidic specie – POPC in the presence of 3 mol% of LW21B (light blue). In this batch, POPC with 25 mol% cholesterol vesicles contained a small impurity (above 1 μm). This impurity is insignificant, since the main peak represents 99,5 % of area under the curve (see **Tab. 7**, p. 37). The width of size distributions of prepared LUVs varies between the compositions (see PdI in **Tab. 7**, p. 37). Concentration of prepared vesicles is also variable (**Tab. 7**, p. 37). Surprisingly, the LUVs with DPPC and cholesterol show almost identical count rates as a control consisting of DOPC. The rest of the LUVs in the batch displays count rates ~2-times lower.

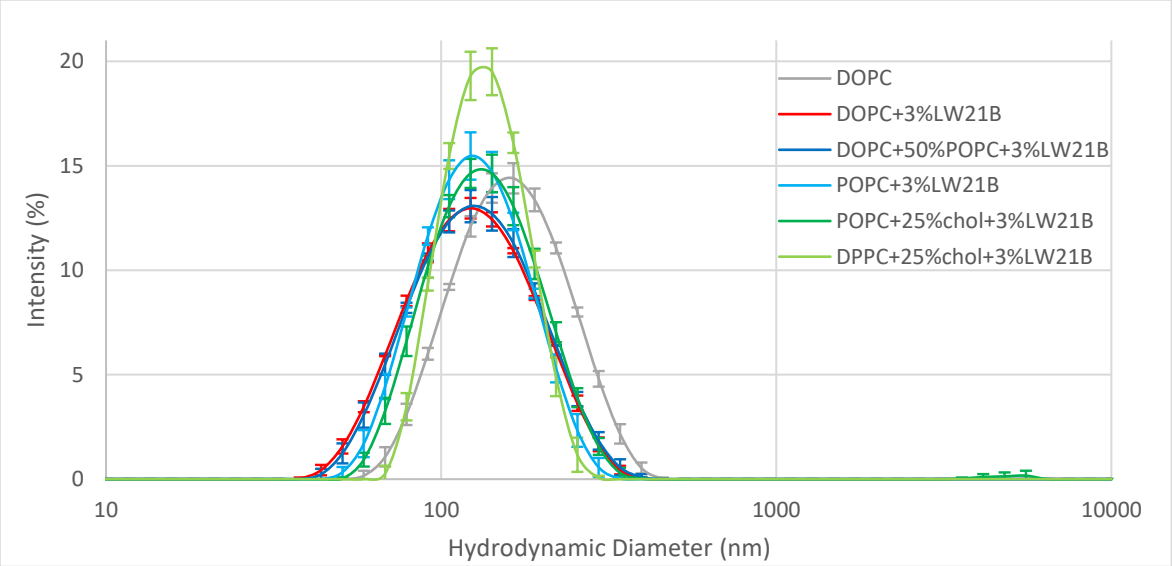

Fig. 15 Size distribution of LUVs with increased saturation of acyl chains measured by DLS. Liposomes containing DOPC only are depicted in grey. Peptide content in remaining LUVs was 3 mol% of LW21B with following lipid composition: DOPC (red), DOPC with 50 mol% POPC (blue), POPC (light blue), POPC with 25 mol% cholesterol (green) and DPPC with 25 mol% cholesterol (light green).

Tab. 7 Quantitative analysis of DLS measurements performed on liposomes with increased saturation of acyl chains. All parameters were gained/calculated automatically using Zetasizer software from three measurements. Size distribution of the vesicles is plotted in **Fig. 15**.

Vesicular Composition	Peak Mean (d. nm)	Peak Area (%)	PdI	Derived Count Rate (kcps)
DOPC	170,8	100	0,130	5,08E+04
DOPC+3%LW21B	134,0	100	0,148	2,62E+04
DOPC+50%POPC+3%LW21B	136,8	100	0,156	2,51E+04
POPC+3%LW21B	132,6	100	0,118	2,54E+04
POPC+25%chol+3%LW21B	142,7	99,5	0,131	2,61E+04
DPPC+25%chol+3%LW21B	139,3	100	0,063	5,03E+04

5.1.4 DLS analysis of LUVs with oxidised phospholipids

In this section, the results of DLS quality control of LUVs containing truncated oxidised phospholipid PGPC are discussed. This batch of liposomes was prepared only in the presence of LW21B peptide.

The size distribution plots of this batch measured by DLS are in **Fig. 16** (p. 38). As for all LUV preparations, this batch contains control LUVs (liposomes consisting only of DOPC) plotted in grey and the reference composition with 3 mol% of LW21B peptide incorporated in DOPC (plotted in red). The rest of model membranes contained 3 mol% of LW21B with alternating lipid composition. Truncated oxidised phospholipids are represented by 10 mol% of PGPC in the presence of either DOPC (blue) or POPC (light blue). Additionally, the combined effect of cholesterol and oxidised lipids was tested. LUVs consisting of 10 mol% of PGPC, 25 mol% of cholesterol and DOPC (green) or POPC (light green) were prepared in this batch of vesicles. Parameters of DLS measurement are summarised in **Tab. 8** (p. 38). Mean hydrodynamic diameter ranges from 126,0 nm for the reference LUVs up to 158,2 nm for the control DOPC vesicles (see **Tab. 8**, p. 38). All compositions display only one distribution peak, highlighting the successful formation of vesicles. The width of distribution (PdI) ranges from 0,053 for POPC, PGPC, cholesterol and peptide containing LUVs up to 0,176 for the reference LUVs with DOPC and peptide (see **Tab. 8**, p. 38). Derived count rate is the highest for the DOPC control and the lowest for the reference control, i.e. approximately 3-times lower than the DOPC control. Concentration of LUVs with the remaining compositions is roughly 2-times lower in comparison to the DOPC control. Only exception is the composition with POPC, PGPC and cholesterol that displays count rates ~1,5-times lower than DOPC only LUVs (see **Tab. 8**, p. 38).

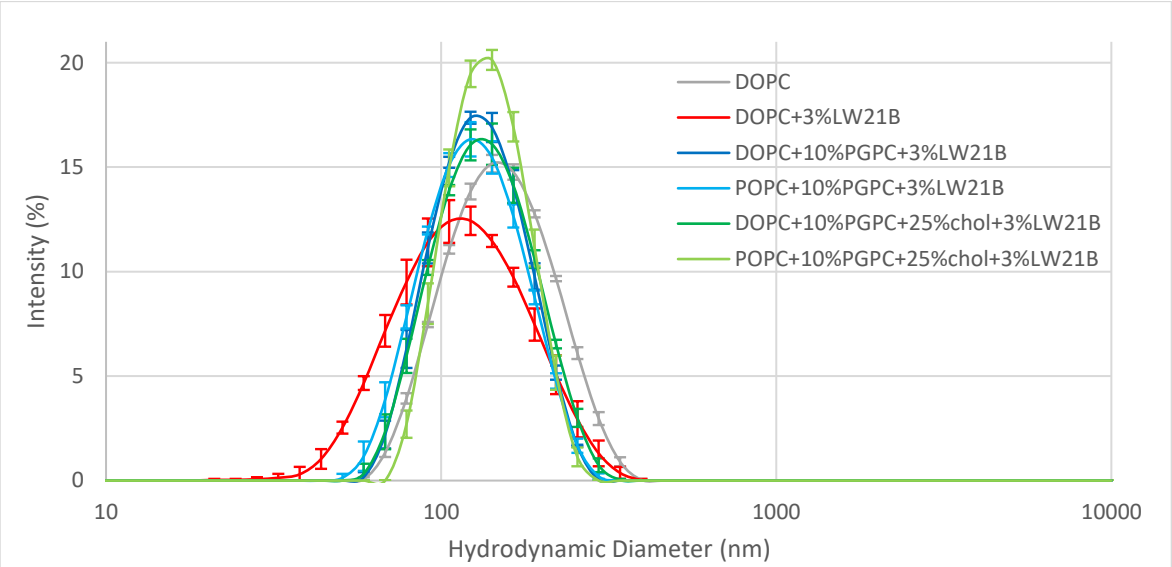

Fig. 16 Size distribution of LUVs containing oxidised phospholipid PGPC measured by DLS. Liposomes containing DOPC only are depicted in grey. Peptide content in remaining LUVs was 3 mol% of LW21B with following lipid composition: DOPC (red), DOPC and 10 mol% of PGPC (blue), POPC and 10 mol% of PGPC (light blue), DOPC with 10 mol% PGPC and 25 mol% of cholesterol (green), POPC with 10 mol% PGPC and 25 mol% of cholesterol (light green).

Tab. 8 Quantitative analysis of DLS measurements performed on liposomes containing oxidised truncated phospholipid PGPC. All parameters were gained/calculated automatically using Zetasizer software from three measurements. Size distribution of the vesicles is plotted in **Fig. 16**.

Vesicular composition	Peak Mean (d. nm)	Peak Area (%)	PdI	Derived Count Rate (kcps)
DOPC	158,2	100	0,108	6,16E+04
DOPC+3%LW21B	126,0	100	0,176	2,26E+04
DOPC+10%PGPC+3%LW21B	135,4	100	0,085	3,21E+04
POPC+10%PGPC+3%LW21B	131,3	100	0,091	2,88E+04
DOPC+10%PGPC+25%chol+3%LW21B	140,8	100	0,097	3,39E+04
POPC+10%PGPC+25%chol+3%LW21B	141,1	100	0,053	4,24E+04

5.1.5 DLS analysis of LUVs with different membrane thickness

Liposomes containing 1,2-dinervonoyl-sn-glycero-3-phosphocholine (24:1PC) were used as a model membrane with much higher thickness compared to the one composed of DOPC only. LW21B peptide was incorporated into LUVs with 24:1PC.

Size distribution of LUVs containing 24:1PC is plotted in **Fig. 17** (p. 39). Grey curve displays distribution of liposomes control. Reference control, containing 3 mol% of LW21B in DOPC is plotted in red and LUVs with 3 mol% LW21B incorporated in a thicker bilayer composed of 24:1PC are in blue. **Tab. 9** (p. 39) contains parameters of plotted curves with

the additional information about this LUV batch. As in all compositions, control LUVs have the highest mean hydrodynamic diameter, with 24:1PC containing vesicles being slightly smaller. Only one distribution peak was observed in all compositions. The width of distribution of 24:1PC containing LUVs is the smallest with the lowest PdI. Relatively high concentration of vesicles composed of 24:1PC was found. These LUVs were prepared in duplicate. In one of these LUVs, the recorded count rate was higher than for the LUVs control. The reference LUVs displayed count rates ~3-times lower compared to the control.

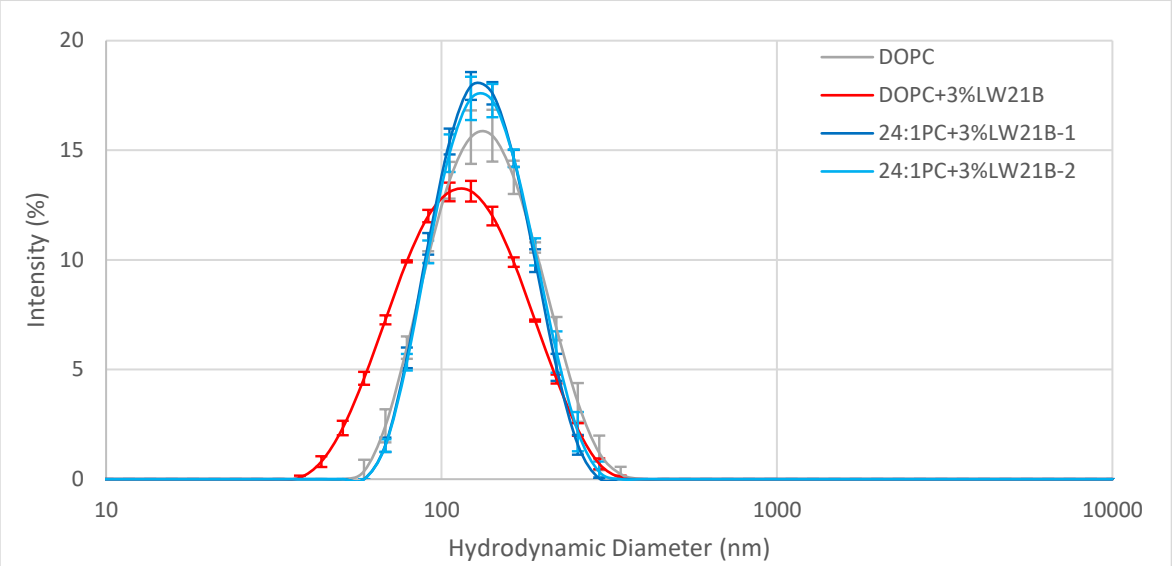

Fig. 17 Size distribution of LUVs with bilayer composed of 24:1PC measured by DLS. Liposomes containing DOPC only are depicted in grey. Peptide content in remaining LUVs was 3 mol% of LW21B with following lipid composition: DOPC (red), 24:1PC (blue and light blue).

Tab. 9 Quantitative analysis of DLS measurements performed on liposomes containing 24:1PC. All parameters were gained/calculated automatically using Zetasizer software from three measurements. Size distribution of the vesicles is plotted in **Fig. 17**.

Vesicular Composition	Peak Mean (d. nm)	Peak Area (%)	PdI	Derived Count Rate (kcps)
DOPC	142,7	100	0,096	6,85E+04
DOPC+3%LW21B	123,1	100	0,154	2,64E+04
24:1PC+3%LW21B-1	135,2	100	0,074	6,98E+04
24:1PC+3%LW21B-2	135,2	100	0,073	5,90E+04

DLS curves show successful preparation of LUVs for all planned compositions with the absence or the presence of minor impurities.

5.2 Analysis of transmembrane peptide aggregation

The previous work in our laboratory demonstrated that LW21A peptide incorporated in LUVs containing DOPC only did not form aggregates in a concentration range 1-5 mol%. The difference in time resolved anisotropy of Trp was tested for a monomeric control (commercially available synthetic melittin), dimeric control (oxidised Cys-LW21) and indicated concentration rage of LW21. Dimeric state of Cys-LW21 peptide was confirmed by mass spectrometry prior to the measurements. Results of the study are shown in **Fig. 18**. Time resolved anisotropy of Trp decays faster in LUVs containing dimeric peptide, while decays of LW21A in a given range of concentration are similar to the monomeric control[24].

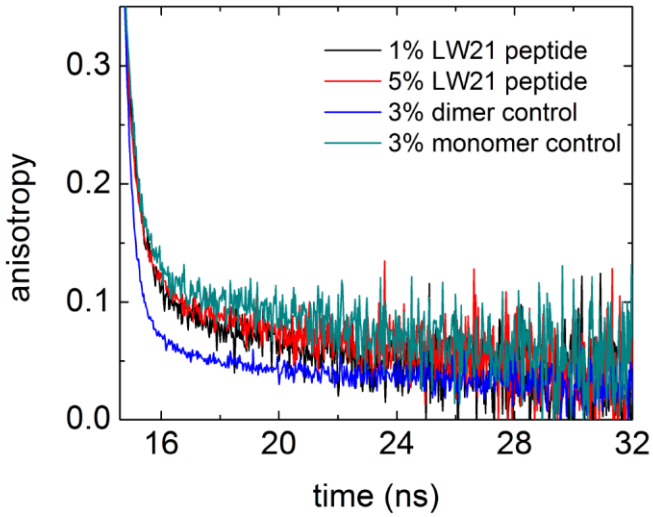

Fig. 18 Time resolved anisotropy decays used as a reference for this thesis. Data show the difference in time resolved anisotropy decays of synthetic peptides according to their aggregation state. These results confirm monomeric state of LW21A peptide (in legend referred to as LW21) in model membrane composed of DOPC. Following controls of aggregation states were used: monomeric – melittin; dimeric – oxidised Cys-LW21. Data were NOT acquired in this thesis and are shown for illustration with the approval of the authors[24].

Based on these results, we decided to use DOPC vesicles with 3 mol% of LW21A as a monomeric control or ones with 3 mol% of oxidised Cys-LW21 as a dimeric control. Even though, results in a **Fig. 18** were published recently they were acquired several years ago. Because of that, mass spectrometry analysis of used peptides was performed prior to the work on this thesis as described in methods. The MS analysis shown degradation of Cys-LW21 peptide. Therefore, it could not be used as a dimeric control in this work. The MS analysis confirmed amino acid composition of the LW21A and LW21B peptides. The measurement and analysis of MS were performed by Zdeněk Kukačka and are not shown.

Due to the results of MS analysis, only monomeric control was available. However, anisotropy curves measured in lipid composition with known aggregation state can be used

as a reference. Increased or decreased level of peptide aggregation can be determined from upper or lower shift of calculated anisotropy decays compared to the reference sample. Therefore, LUVs containing 3 mol% of the peptide in DOPC only were used as the reference control for all time resolved anisotropy measurements. The critical condition for such comparative analysis is that measurements are performed under the same conditions. Small changes in the instrument setup can lead to the results with minor differences, but since changes in anisotropy are always very small in absolute numbers, the setup of the instrument (polarizers, position of cuvette, lens…) must be maintained identical for the samples that are directly compared. As described in the methods section, Trp is not the ideal fluorophore and even with the mentioned compromises in the form of lowered resolution, measurement of one sample usually takes several hours. This limits the number of measured samples compared within a batch.

5.2.1 The electrostatic effect of charged amino acid residues

As mentioned in the methods part, LW21B peptide was designed with adjusted amino acid sequence in comparison to LW21A (**Tab. 1**, p. 24). The changes led to the neutralisation of the charges in the part of the peptide at the water-bilayer interface. To verify the behaviour of the LW21B peptide, time resolved anisotropy decays of both peptides have been compared after incorporation into LUVs consisting of DOPC (**Fig. 19**, p. 42). Duplicate LUVs with the same composition have been prepared and analysed. Anisotropy decays of Trp fluorescence in model membranes with 3 mol% of LW21A are plotted in red and the ones with 3 mol% of LW21B in blue. Shortly after the excitation, very fast decay of anisotropy is visible (14-15 ns). High values of anisotropy at the beginning of decays are the result of light scattering. Because Trp is a very weak fluorophore, small amount of scattered light can already distort the decay curves. The reason for light scattering is the presence of large objects, LUVs. Fast decay after the excitation is visible in all measured decays. Luckily, the scattering only distorts beginning of the decay curves and the fluorescence anisotropy can be determined from the remaining part of curves. In **Fig. 19** (p. 42), change in anisotropy decays between LUVs with different composition is noticeable. However, it decays faster in LUVs with LW21B peptide. This implies that LW21B forms clusters in very fluid membranes composed of only DOPC. As mentioned before, such behaviour has not been observed for LW21A with high positive charge at the lipid-water interface. The result suggests a potential role of electrostatic repulsion in the aggregation of TMD domain.

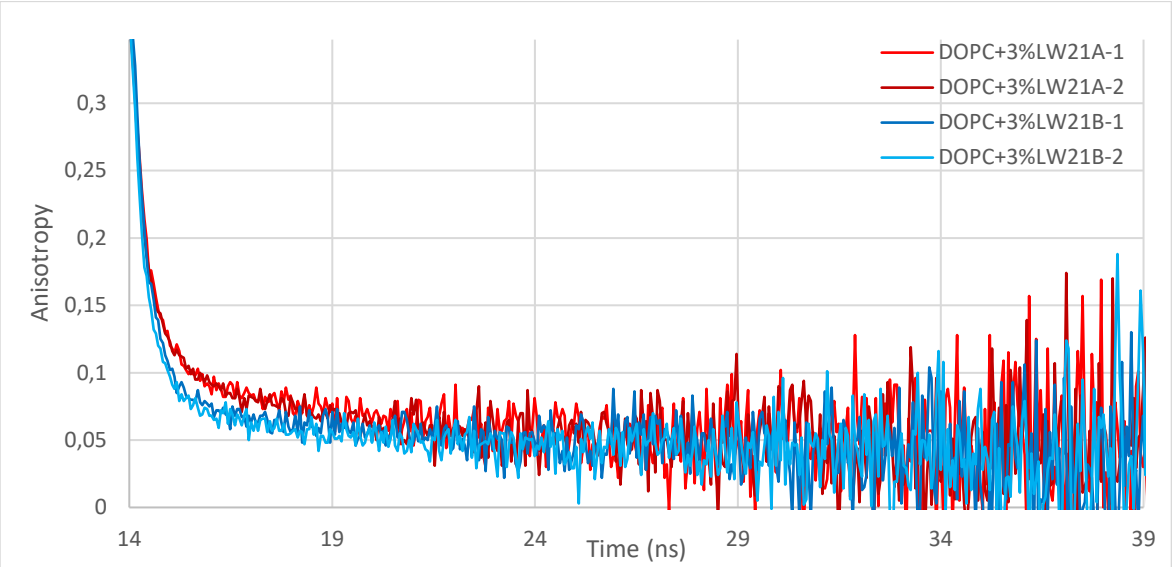

Fig. 19 The peptides with diverse electrostatic properties of flanking amino acids exhibit different levels of clustering in model membranes. Time resolved anisotropy decays of Trp for LW21A and LW21B. All liposomes contained only DOPC as lipidic species.

5.2.2 The effect of membrane thickness

In the previous section we confirmed that two peptides LW21A and LW21B differ in their clustering properties. As mentioned in the methods section, the amount of available LW21A peptide was limited and LW21B had to be used for a majority of experiments. Therefore, we decided to test if the higher extend of time resolved anisotropy change could be displayed by LW21B under conditions of exchanged membrane thickness.

Clustering of transmembrane peptides similar to ours was reported in the membranes with negative hydrophobic mismatch[36]. This is the case when membrane is thicker than TMD of embedded protein or peptide. In model membranes, thickness is controlled by the phospholipids with fatty acyl chains of a specific length. In our case, we employed LUVs consisting of 1,2-dinervonyl-sn-glycero-3-phosphocholine (24:1PC). The peptide with similar amino acid composition as used in this thesis was reported to incorporate well into the bilayer with only 24:1PC phospholipid[28]. Difference in the aggregation of LW21B in DOPC and 24:1PC was tested.

Anisotropy decays for the two compositions are plotted in **Fig. 20** (p. 43). Red curve represents the reference anisotropy decay of LW21B Trp measured in LUVs containing DOPC only. Anisotropy decay from a thick bilayer formed by 24:1PC is plotted in blue. It can be noticed that anisotropy decays to slightly lower values for the peptide in thicker membranes when comparing the curves in **Fig. 20** (p. 43) between 15-19 ns. This implies formation of a higher number of clusters or the more favourable orientation of LW21B Trp

residues for homo-FRET. Even though anisotropy curve for the thicker membrane is noisy, it shows, that small changes can be still detected. This result also confirms that for the studies of the impart of LW21B in DOPC containing LUVs can be used as a reference lipid composition on peptide clustering.

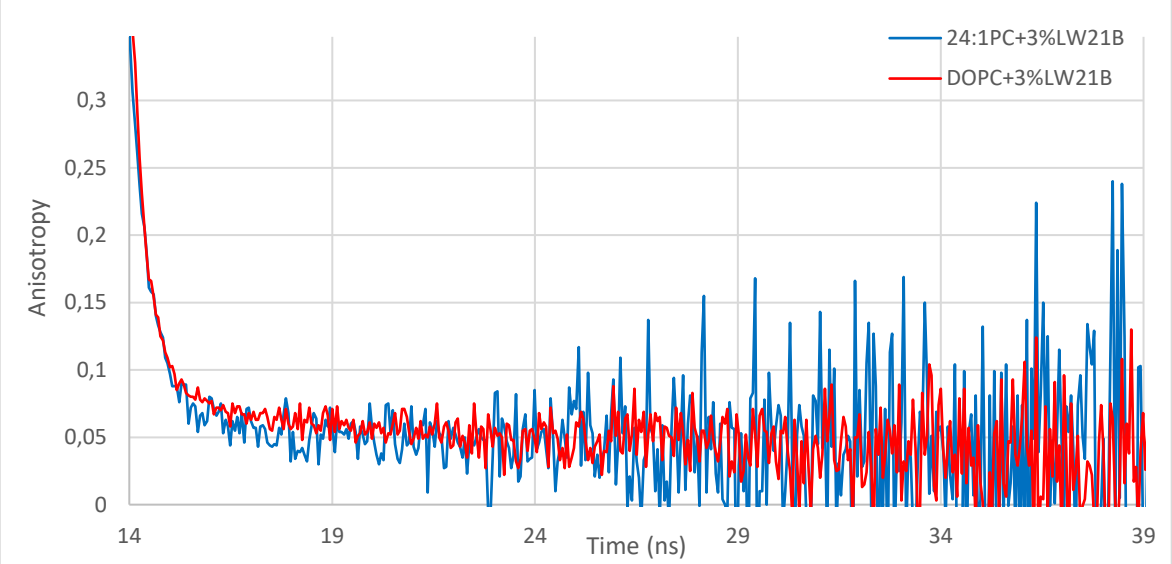

Fig. 20 Negative hydrophobic mismatch leads to change in clustering of LW21B peptide. Comparison of anisotropy decays of LW21B Trp measured with and without negative hydrophobic mismatch. Blue curve represents decay from bilayer with the mismatch. Reference composition with DOPC is present in red. Both compositions contained same amount of LW21B peptide (3 mol%).

5.2.3 The effect of palmitic acid

Cells cultivated with palmitic acid (PA) activate UPR pathway even in cells where the native TMD of IRE1 was exchanged for polyLeu stretch and their luminal domain is incapable of sensing unfolded proteins[60]. One of the possible explanations is, that PA incorporates into membranes of the cell, in this case of the ER. The presence of PA in membranous structures results in increased membrane rigidity due to its saturated alkyl chain.

Liposomes composed of DOPC with 10 mol% of PA were prepared in the presence of 3 mol% of LW21A or LW21B peptide. Time resolved anisotropy curves were calculated from measured VV and VH fluorescence decays and compared with anisotropy decays measured in LUVs with reference composition consisting of DOPC and 3 mol% of LW21A or LW21B. Time resolved anisotropy decays are compared in **Fig. 21** and **Fig. 22** (p. 44). In both figures, reference composition is represented by red decay curve. Anisotropy decays for LUVs with PA in both figures are plotted in blue. No difference in time resolved decays of anisotropy was observed in the presence of PA compared to the reference composition.

Therefore, no change in clustering of LW21A or LW21B peptides occurs when 10 mol% of PA was incorporated in the DOPC membranes.

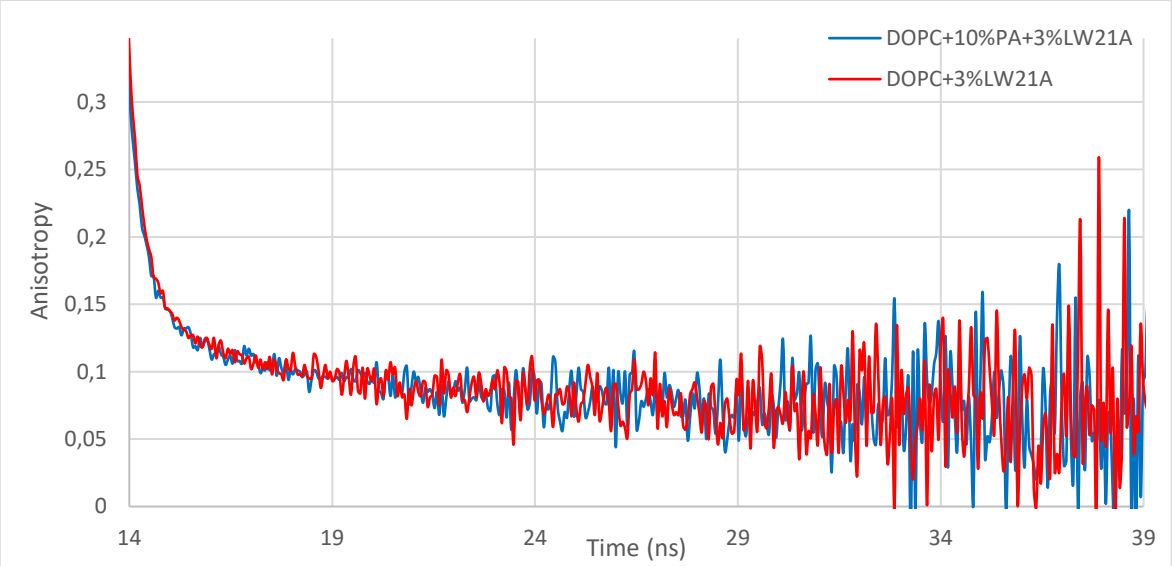

Fig. 21 Palmitic acid has no effect on LW21A clustering. Time resolved anisotropy decays of Trp in LW21A peptide do not differ when incorporated into liposomes with or without PA. All liposomes contained 3 mol% of LW21. Red decay curve of anisotropy is plotted for the reference control composition containing DOPC only and blue for liposomes with 10 mol% of PA.

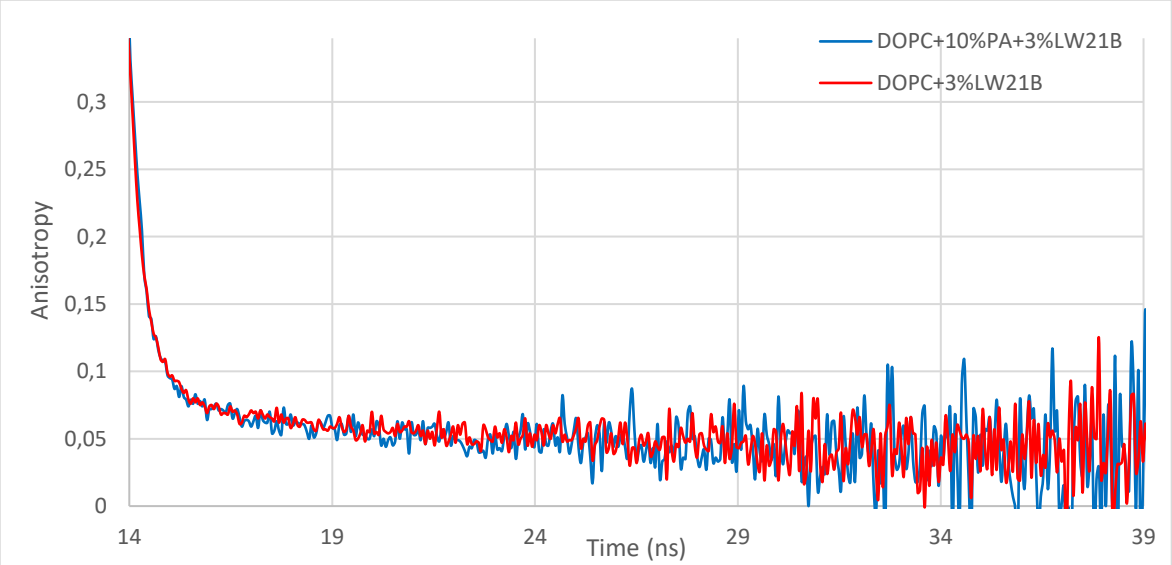

Fig. 22 Palmitic acid has no effect on LW21B clustering. Time resolved anisotropy decays of Trp in LW21B peptide do not differ when incorporated into liposomes with or without PA. All liposomes contained 3 mol% of LW21B. Red decay curve of anisotropy is plotted for the reference control composition containing DOPC only and blue for liposomes with 10 mol% of PA.

5.2.4 The effect of cholesterol

Increased cholesterol in a diet of cultured cells has been known to induce the ER stress, leading to UPR[55]. In a membrane, molecules of cholesterol act as a buffering agent that rigidifies a highly mobile membranes and in some other case, it keeps highly rigid

membranes still in fluid state. In this case, introduction of cholesterol into liposomes containing DOPC rigidifies model membrane which could lead to changes of time resolved fluorescent anisotropy for synthetic model peptides LW21A or LW21B.

Time resolved anisotropy decays were measured in reference control containing DOPC and 3 mol% of either LW21A or LW21B. These decays were compared to the measurements obtained with LUVs composed of DOPC, 25 mol% cholesterol and 3 mol% of LW21A or LW21B. Comparison of anisotropy decays is shown in **Fig. 23** for LW21A peptide and in **Fig. 24** (p. 46) for LW21B peptide. In both figures, red curve corresponds to the anisotropy decay of reference control and blue one represents cholesterol-containing LUVs. In both figures, no difference in anisotropy decay could be seen when reference composition is compared to cholesterol containing LUVs. This indicates that no detectable change in aggregation occurs in the presence of cholesterol.

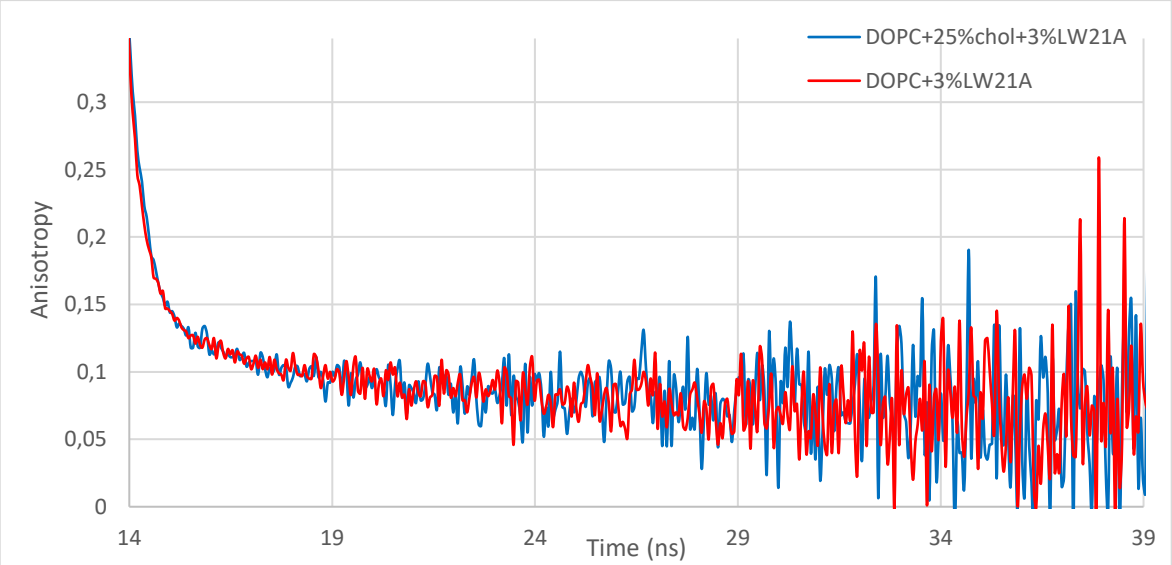

Fig. 23 Cholesterol has no effect on clustering of LW21A peptide. Time resolved anisotropy decays of Trp in LW21A peptide do not differ when peptide incorporates into liposomes with or without cholesterol. All liposomes contained 3 mol% of LW21. Red decay curve of anisotropy is plotted for the reference control containing DOPC as the only lipidic moiety and blue for LUVs with 25 mol% of cholesterol.

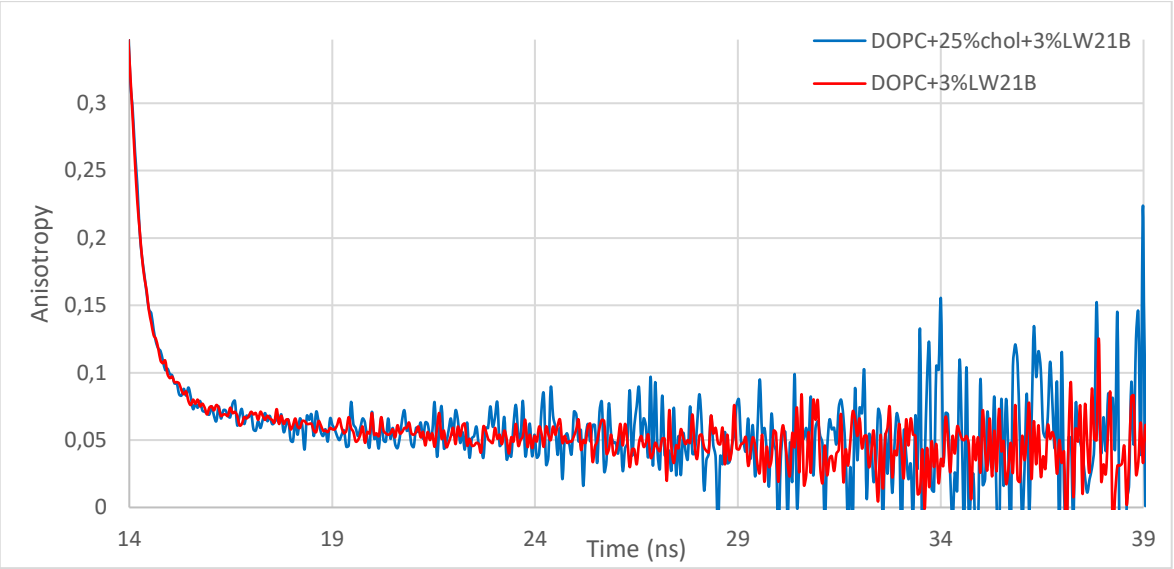

Fig. 24 Cholesterol has no effect on clustering of LW21B peptide. Time resolved anisotropy decays of Trp in LW21B peptide do not differ when peptide incorporates into liposomes with or without cholesterol. All liposomes contained 3 mol% of LW21B. Red decay curve of anisotropy is plotted for the reference control containing DOPC as the only lipidic moiety and blue for LUVs with 25 mol% of cholesterol.

As described in the methods section, the available amount of LW21A peptide was sufficient only for three tests. These results are shown in previous sections and indicated comparable sensitivity of the peptides for changes in membrane environment. The remaining measurements were performed using LW21B peptide.

5.2.5 The effect of saturated fatty acyl chains

The addition of PA to model membranes may not perfectly mimic its effect on cellular membranes when added to a culture media. In cells, PA can be metabolised and incorporated into phospholipids. Because of that, we also tested peptide aggregation in lipid compositions containing phospholipids with saturated fatty acyl chains.

Glycerophospholipids are the most abundant lipid species of biological membranes in animal cells[6]. Therefore, their fatty acyl chains can significantly influence properties of cell membranes. For example, membrane rigidity can be modified by exchanging the fatty acyl chains. In our reference composition, DOPC is used as a sole lipid. If one of DOPC's fatty acyl chains is exchanged for a saturated palmitate, phospholipid POPC emerges, and in case when both fatty acyl chains of DOPC are exchanged for palmitate, it is DPPC. Both of phospholipids with higher degree of saturation in their fatty acyls increase the rigidity of membranes. This could lead to a change in aggregation of peptides or proteins embedded in the membrane.

Liposomes containing 3 mol% of LW21B in DOPC were used as reference control and compared to the LUVs containing varying amount of POPC to probe the effect of increased presence of saturated fatty acyl chains in membranes on the peptide clustering. In this part, DPPC could not be tested due to its high transition temperature (41°C) which would cause the formation of S_o phase membranes. To overcome the formation of solid phase in DPPC containing membranes, cholesterol was used and the results are discussed in the next section. Thickness of membranes consisting of POPC or DOPC is similar. Thus, no loss of peptide incorporation or a change in the aggregation due to the hydrophobic mismatch is expected. Time resolved anisotropy curves of reference control (red), LUVs with 50 mol% of POPC (blue) and POPC only (green) are plotted in **Fig. 25**. All model membranes contained the same amount of LW21B peptide (3 mol%). No difference between plotted time resolved anisotropy decays was found (see **Fig. 25**). Therefore, we conclude that there is no change in the peptide aggregation in membranes containing phospholipids with increasing content of saturated fatty acyl chains.

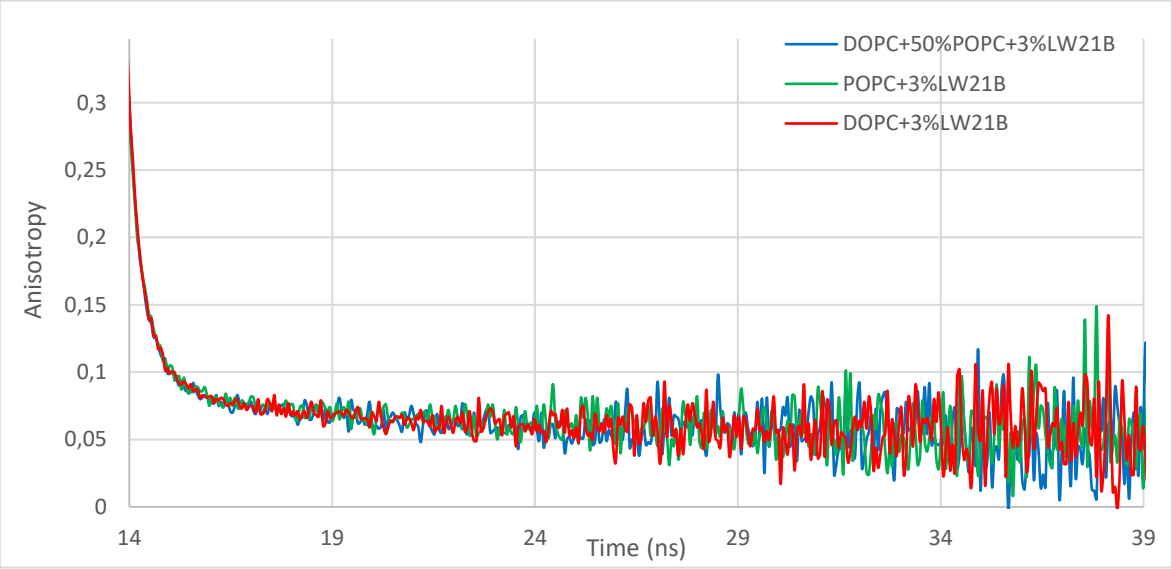

Fig. 25 Saturation of PC's fatty acyl chains does not change clustering of LW21B. Time resolved anisotropy decays of Trp in LW21B peptide do not differ when incorporated into LUVs with increased fatty acyl chain saturation. All liposomes contained 3 mol% of LW21B. Red anisotropy decay curve is plotted for reference control containing only DOPC, blue for LUVs with DOPC and 50 mol% POPC and green for ones containing only POPC.

5.2.6 Combined effect of cholesterol and saturated fatty acyl chains

In previous sections, separate effects of cholesterol and saturated fatty acyl chains were studied and no detectable changes in time resolved anisotropy were found. We further tested whether the combined effect of saturated fatty acyls and cholesterol on membrane properties

could lead to a change in aggregation of peptides. In living cells, these membrane components always coexist.

Results of anisotropy decays in LUVs with two different lipidic compositions were compared to our established reference control (plotted in **Fig. 26**). In both cases, 25 mol% of cholesterol was added to LUVs with different composition of phospholipid fatty acyl chains. As previously mentioned, one of the compositions contained phospholipid with both saturated fatty acyl chains (DPPC; green decay in **Fig. 26**). The second LUVs contained phospholipid with one saturated and one unsaturated acyl chain – POPC (plotted in blue in **Fig. 26**). Comparison of curves shows only a modest difference in the short times after the excitation. However modest, the differences are well detectable when compared to the reference composition and the measurements where saturated acyl chains and cholesterol were tested separately. Therefore, we conclude that slight changes in the aggregation can be observed in these highly rigidified membranes.

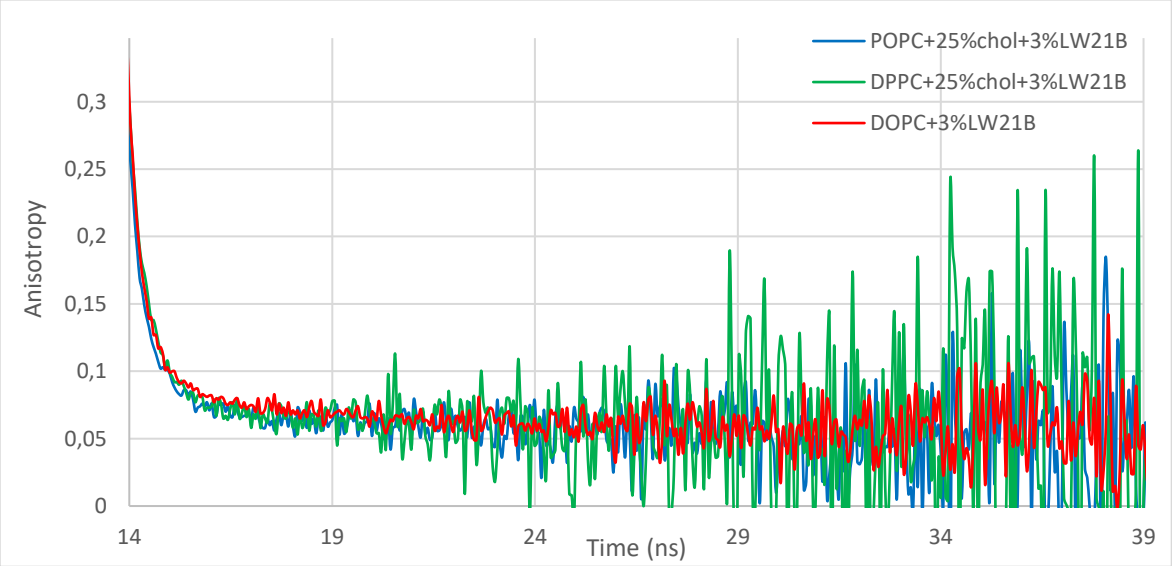

Fig. 26 Combined effect of saturated fatty acyls and cholesterol on clustering of LW21B peptide. Time resolved anisotropy decays of Trp in LW21B peptide slightly vary when incorporated into LUVs with combined presence of cholesterol and saturated fatty acyl chains. All liposomes contained 3 mol% of LW21B. Red decay curve of anisotropy is plotted for reference control containing DOPC only, blue for LUVs with POPC as a main phospholipid with addition of 25 mol% cholesterol and green for DPPC with 25 mol% cholesterol.

5.2.7 The effect of oxidised phospholipids

Oxidised phospholipids have been recognised as members of both physiological and pathological processes in living cells[79]. Increased mobility of lipids in model systems with truncated phospholipid PGPC has been reported[39]. Therefore, we wanted to test whether the presence of PGPC can affect peptide aggregation when compared to the reference control.

Model membranes with 10 mol% of PGPC were prepared in order to probe the change in LW21B aggregation in LUVs containing the truncated oxidised phospholipid. LUVs with POPC as a main lipidic component has been prepared as well. The results of time resolved anisotropy are plotted in **Fig. 27**. Reference control composed of DOPC and 3 mol% of LW21B is plotted in red. Decays of Trp anisotropy for LUVs containing 3 mol% of LW21B, 10 mol% of PGPC and either DOPC or POPC are plotted in blue or green, respectively. Anisotropy decays calculated from the measurements in LUVs containing PGPC do not differ from those for the reference composition. Thus, the presence of 10 mol% PGPC has no effect on the aggregation of embedded LW21B peptides.

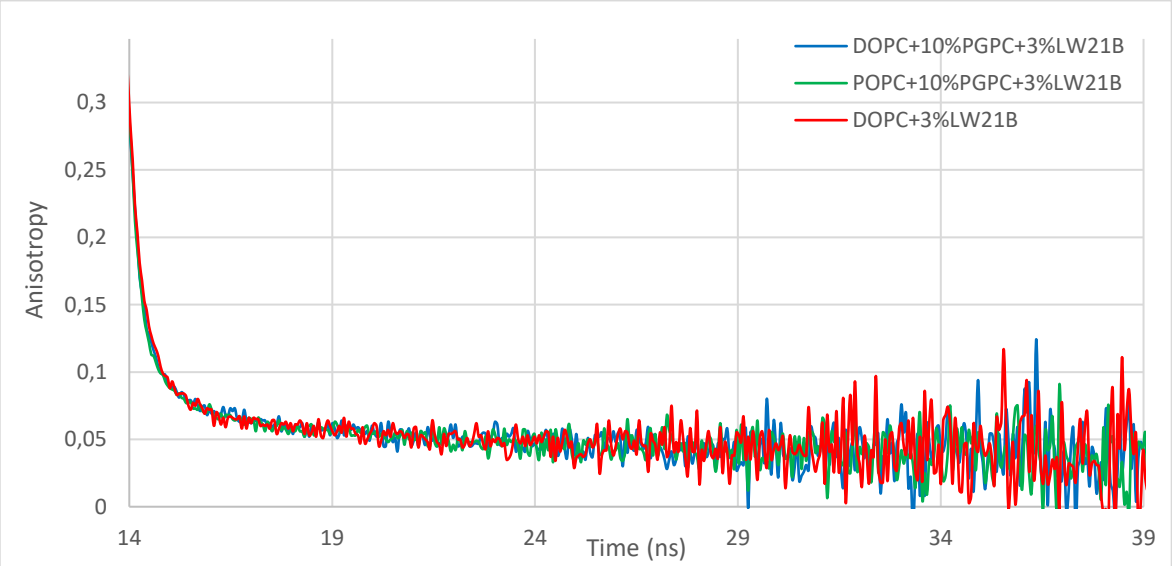

Fig. 27 Oxidised phospholipid PGPC has no effect on LW21B clustering. Time resolved anisotropy decays of Trp in LW21B peptide does not differ when incorporated into LUVs with PGPC, containing truncated oxidised fatty acyl chain. All liposomes contained 3 mol% of LW21B. Red decay curve of anisotropy is plotted for reference control containing DOPC only, blue for LUVs containing DOPC with 10 mol% of PGPC and green for LUVS with POPC as a main phospholipid with the addition of 10 mol% of PGPC.

5.2.8 Combined effect of oxidised phospholipids and cholesterol

Cholesterol and oxidised phospholipids simultaneously coexist in membranes of cells that undergo oxidative stress. Combination of these two components in model membrane systems has been reported to "heal" membranes. In the presence of truncated oxidised phospholipid, cholesterol can fill the void volumes formed by a missing fatty acyl chain leading to the improvement in membrane properties and closer resembling of the physiological conditions[38]. Therefore, we aimed to test the combined effect of cholesterol and truncated PGPC on the aggregation of LW21B peptide.

Based on the previous experiment, LUVs with 10 mol% of PGPC were used for comparison. Additionally, 25 mol% of cholesterol has been added. Base lipids were either DOPC or POPC, with all the compositions containing 3 mol% of LW21B peptide. Time resolved anisotropy decays for the comparison of peptide aggregation in the presence of truncated lipids and cholesterol are plotted in **Fig. 28**. The decay for the reference composition is plotted in red. LUVs containing DOPC as a main lipidic component are in blue and the ones with POPC are plotted in green. No differences in time resolved anisotropy decays were observed. Therefore, we conclude that the presence of oxidised truncated phospholipid PGPC and cholesterol does not affect peptide behaviour in synthetic membranes.

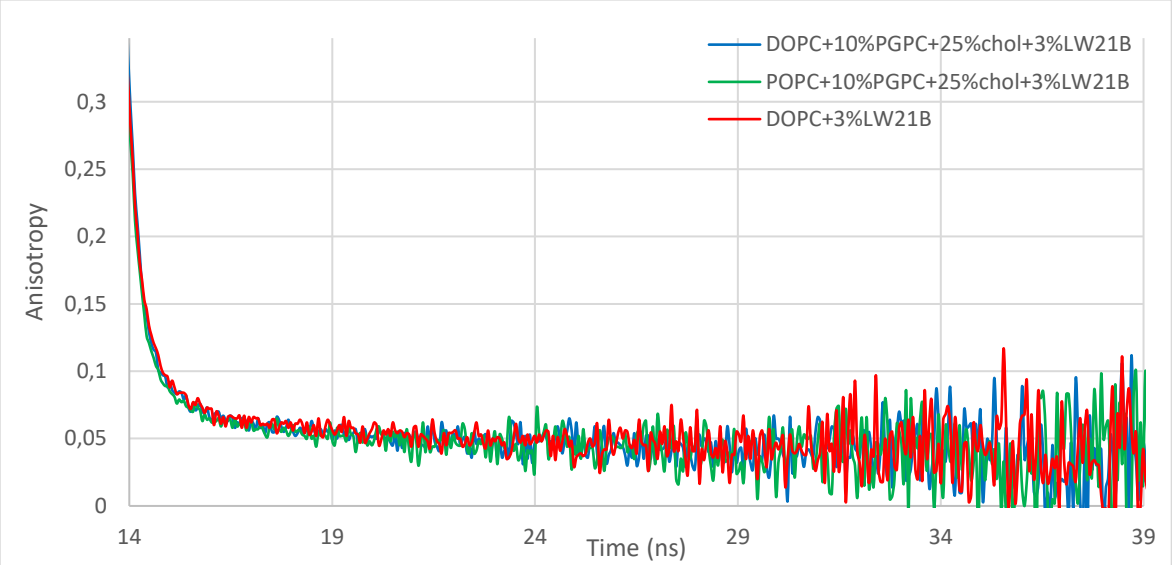

Fig. 28 Combined effect of oxidised phospholipid PGPC and cholesterol does not change the aggregation of LW21B peptide. Time resolved anisotropy decays of Trp in LW21B peptide does not differ when incorporated into LUVs with PGPC and cholesterol. All liposomes contained 3 mol% of LW21B. Red decay curve of anisotropy is plotted for the reference control containing DOPC only. Remaining compositions contained 10 mol% of PGPC with 25 mol% of cholesterol in the presence of either DOPC (blue) or POPC (green).

6 Discussion

Several proteins capable of sensing changes in membrane properties have been described in parts[62]. Among those, IRE1 is the best described signalling protein connected to the recognition of unfolded proteins in the ER[45]. The presence of unfolded proteins in the ER leads to a complex cell response called unfolded protein response (UPR). UPR is also connected to the activation of genes responsible for lipid biosynthesis, metabolism and homeostasis[57]. This led to the discovery of the IRE1 ability to sense lipid-induced imbalance[55,57,58]. Mechanism of IRE1 activation by unfolded proteins is well established[48]. For the lipid-induced activation of IRE1 were reported ambiguous results[60,61]. One of these studies shows that IRE1 can sense the lipid-induced ER stress also when anchored to the ER membrane by a TMD with unspecific amino acid sequence. Such a conclusion was obtained by the replacement of IRE1 TMD with the artificial polyLeu amino acid sequence. Similar to the native form, IRE1 with polyLeu TMD was activated upon the addition of PA to the medium with cultured cells[60]. One of the possible explanations is that PA enters membranes of cultured cells, where it causes change in the overall ER membrane properties. It was hypothesised that such a change in membrane properties can induce aggregation of IRE1 via its TMD[58]. To address the question whether aggregation of polyLeu TMD can be induced by changes in membrane lipid composition, i.e. membrane biophysical properties, we employed model membranes in form of LUVs with incorporated synthetic transmembrane peptides. Lipidic composition of LUVs was designed to modify membrane properties of this model system. Transmembrane peptides used in this work contain Trp residues at the water-bilayer interface (for exact sequence, see **Tab. 1**, p. 24). The fluorescent properties of Trp can be used for spectroscopic studies. We employed time resolved anisotropy which provides information about the occurrence of homo-FRET as shown before[24]. Therefore, we gained a system to address on our desired question by using Trp residues as a fluorophores and homo-FRET as indicator of aggregation. Importantly, our model system did not require conjugation of peptides to bulky synthetic fluorophores.

In the first part of this thesis, formation of LUVs by extrusion was performed. DLS was employed to the verify formation of LUVs of a desired size. Results are summarized in section 5.1. Model membranes with all compositions displayed hydrodynamic diameter larger than the pore size of the membrane filter used for extrusion. This has been reported in the past for LUVs prepared by the repeated extrusion of MLVs through a polycarbonate membrane[78,80]. Because MLVs are repeatedly forced to pass pores smaller than their

diameter, they undergo some degree of deformation. After the passage of model membranes through the membrane filter, vesicles can regain spherical shape that is bigger than the pores of the filter[80]. Sizes of prepared vesicles slightly varied depending on the lipid composition. LUVs in the presence of peptides display lower hydrodynamic diameter in comparison to the control LUVs that contained only DOPC. It is tempting to conclude that LUVs with lipidic compositions leading to the formation of membranes with high elasticity can be compressed more during the passage through the membrane filter in the absence of vesicular break-down. This behaviour of LUVs has been reported for vesicles containing cholesterol[81]. However, it was also shown that the size of LUVs prepared by the extrusion significantly depends on pressure[80,81]. In this work, the extrusion was performed manually, i.e. poor control of applied pressure. Therefore, the composition-dependent size of LUVs is probably a coincidence. However, pressure-dependent size of LUVs can explain a high variability of hydrodynamic diameter measured for the DOPC only and reference controls in separate batches (see **Tab. 4-9**, p. 33-39).

Moreover, higher concentration of LUVs was achieved for vesicles that did not contain peptides (referred to as DOPC control). Derived count rate of scattered light was ~3-times higher for the DOPC control vesicles in comparison to the compositions with incorporated peptide (see **Tab. 4-9**, p. 33-39). It was reported that downsizing of MLVs containing a peptide by the extrusion through porous membranes can lead to a peptide loss[28]. Majority of lost peptide was reported to be located on the porous membrane used for the extrusion[28]. In my bachelor thesis, I tested peptide incorporation into LUVs using semi-quantitative method. The amount of peptide lost in the process of LUVs preparation by the extrusion was analysed by LC-MS technique with the results displaying loss of roughly 25 % of the peptide[82]. Therefore, the peptide loss cannot account for such a big drop in the concentration of LUVs. We speculate that the loss of vesicles in the process of extrusion is due to the failure of MLVs aggregates to disassemble and pass polycarbonate membrane.

A major part of this thesis was focused on the measurements of time resolved anisotropy decays in LUVs containing transmembrane peptides LW21A or LW21B (for their amino acid sequence see **Tab. 1**, p 24). To address the changes in the aggregation state of the peptides, anisotropy decay curves were measured for the reference composition containing DOPC and 3 mol% of LW21A or LW21B. Under these conditions, time resolved anisotropy decayed faster for vesicles with the LW21B peptide (**Fig. 19**, p. 42). As already reported in the past[83], the peptide aggregation depends on the charge of flanking residues surrounding

the hydrophobic part of a TMD. The overall charge of flanking residues is +1 and +3 for N- and C-terminus respectively for LW21A peptide and 0 for both sides in the redesigned LW21B peptide (see **Tab. 1**, p 24). In the above mentioned study, synthetic peptides with flanking residue charge equal to +1 on both sides did not cluster while peptides with neutral charge of flanking residues aggregated[83]. Interesting indications for single spanning proteins can be drawn from these results. It suggests that their tendency to form membrane aggregates can be regulated at the level of amino acid sequence of TMD flanking residues. Therefore, we analysed the amino acid sequence of proteins responsible for the induction of UPR in the UniProt database[84]. The overall charge of four amino acids flanking the transmembrane domain differs between the human UPR transducers (**Tab. 10**, p. 54). ATF6 has the charge of flanking residues on both lumenal and cytosolic side relatively high -2 and +3, respectively. Mechanism of ATF6 activation upon ER stress recognition does not include formation of clusters. Therefore, high electrostatic repulsion could be one of the reasons for its behaviour in the membrane of the ER. However, dimerization or aggregation are involved in the self-activation and the UPR signal transduction induced by both PERK and IRE1 proteins. The charge of flanking residues of PERK on the lumenal side of TMD is +2, while on the cytosolic side charged residues are not present. Therefore, charged residues probably keep the PERK in the monomeric state while the ER is in the physiological conditions. The other interesting feature of the PERK's TMD is a pair of charged amino acids (KE) in the centre of the bilayer. We hypothesize, that these two residues will neutralise themselves in the PERK's monomeric state while if the ER stress occurs, KE pair on each TMD can interact when in the close vicinity, and dimerization and subsequent activation of PERK can occur. IRE1 of yeast also contains charged pair of amino acids in its TMD, which can lead to the activity similar to the human PERK. Another human sensor of the ER stress, IRE1α does not bear the net charge of the flanking residues. Similarly to the results of this study, where peptide LW21B that does not bear any net charge of flanking residues and aggregates already in the fluid DOPC membranes, IRE1α could be the highly sensitive sensor which is "always ready" for the immediate action. This would mean, that IRE1α is the first of the UPR signal transducers activated under the conditions of developing ER stress. In the complex environment of a cell, all of the signal transducers could be also fine-tuned for the cell's signalization requirements by local pH or ion concentration.

Tab. 10 TMD flanking sequences of human ER proteins responsible for the UPR. Flanking residues of four amino acid sequence are shown. The net charge of each flanking side is described. Sequences were acquired from UniProt database[84].

Protein	UniProt Number	Net Charge	LUMENAL flanking sequence	TMD*	CYTOSOLIC flanking sequence	Net Charge
IRE1α	O75460	**0**	ML**KD**		PLSM	**0**
PERK	Q9NZJ5	**+2**	**RKKD**		TTFI	**0**
ATF6	P18850	**-2**	**E**Q**D**S		P**KRR**	**+3**

TMD domain sequence of IRE1α:* MATIILSTFLLIGWVAFIITY*, PERK:* PVLLLHWWK****E**IVATILFCIIA *and ATF6:* VVCVMIVLAFIILNYGPMSML

When hydrophobic mismatch occurs, one of the possible outcomes for the relaxation of the increased energy in a system is clustering of TMD of proteins or synthetic peptides[36]. This was first suggested in so called mattress model of membrane organisation[85]. In our work, we employed the negative mismatch to verify the response of the peptide to such a change in membrane properties. This effect is induced by the incorporation of a peptide into the membrane that is thicker than its hydrophobic length[36]. We have prepared LUVs composed of 24:1PC and 3 mol% of the peptide. Both peptides, LW21A and LW21B were designed to fit perfectly into the DOPC containing membranes (18:1PC). However, it was shown that such peptides can incorporate well into the membranes composed of 24:1PC[28]. Time resolved anisotropy of LW21B peptide in 24:1PC membranes was measured with distinguishable change in aggregation compared to DOPC only reference. However, the signal noisiness of the calculated curve for LUVs with 24:1PC limits our interpretation(s) (see **Fig. 20**, p. 43). In the literature, data indicating peptide aggregation under conditions of negative mismatch measured by both time resolved fluorescence spectroscopy[86] and pulsed electron paramagnetic resonance[87] were reported. Based on our expectations and the previously reported results, we expect that small changes in anisotropy decays report on increased aggregation of LW21B peptide in membranes with negative hydrophobic mismatch. Due to the limited amount of available LW21A peptide, these results could not be repeated with this non-aggregating variant of LW21.

Increased fatty acid saturation in membranes activates IRE1 and PERK[58]. Enzymatic activity of PERK lacking its luminal domain was retained in the proteoliposomes containing saturated phospholipids[58]. Therefore, we tested the effect of increased membrane rigidity on clustering of our transmembrane peptides. Membrane rigidity in a model system was induced by the PA, cholesterol, POPC and DPPC. Individual results of the measurements are described in detail in Results sections 5.2.3-5.2.6. LUVs with incorporated peptides in the

presence of PA, cholesterol or POPC did not display any change in the aggregation state compared to the reference lipid composition (see **Fig. 21-25**, p. 44-47). Minor changes in the aggregation state of LW21B peptide could be detected in LUVs composed of 25 mol% cholesterol and either POPC or DPPC (see **Fig. 26**, p. 48). In the composition with POPC, cholesterol bears a rigidifying function and, in the membranes containing DPPC the function is opposite due to the very high transition temperature of DPPC (41°C). It is interesting that the presence of cholesterol in membranes with POPC does lead to the change in clustering of LW21B peptide, while in composition with DOPC such a change was not distinguishable (see **Fig. 24** and **Fig. 26**, p. 46 and 48). It would be also interesting to compare clustering changes of LW21A peptide, where higher degree of aggregation could be probably recognised. Due to its limited availability, this experiment was not performed.

Recently, the induction of combined oxidative and ER stress by PA was reported in the H9c2 rat cells[88]. Oxidative stress causes formation of oxidised lipidic species in cells[89]. Some of oxidised lipids can accumulate in membranes of the cell – e.g. ER membrane. In our laboratory, the impact of truncated oxidised phospholipids on membrane properties has been studied extensively[38,39,90]. Therefore, the aggregation state of LW21B peptide was also studied in the presence of PGPC with and without cholesterol (sections 5.2.7 and 5.2.8) In both cases no change in aggregation was observed. For details see **Fig. 27**(p. 49) and **Fig. 28** (p. 50) for PGPC and PGPC with cholesterol, respectively. The results with PGPC under herein tested conditions are conclusive. But the clustering of peptides in membranes containing different types of oxidised phospholipids cannot be completely dismissed because of the complexity of molecules originating from oxidative stress in the cells[91]. Therefore, properties of membranes composed of different oxidised phospholipid could theoretically lead to formation of clusters of the transmembrane peptides.

Impact of membrane properties on clustering of synthetic peptides incorporated into model membranes was successfully studied in our system. Increased saturation of phospholipids forming the bilayer and hydrophobic mismatch increase the clustering of these peptides. However from our studies, we conclude that the charge of flanking residues of TMD plays a bigger role than biophysical properties of membrane.

7 Conclusion

This thesis is focused on how changes in membrane biophysical properties may affect clustering of synthetic transmembrane peptides. Using model membranes in form of LUVs, changes in membrane properties were induced in a controlled way by altering their lipid composition. Formation of LUVs was confirmed by DLS and clustering properties of incorporated peptides were analysed using time resolved fluorescence anisotropy. Importantly, the results indicate that a major role in clustering of peptides is the amino acid sequence of residues flanking the hydrophobic part. The difference in aggregation caused by altered membrane properties was at the detection limit of the applied method. Some changes were observed under rather extreme conditions that are usually not found in the biological membranes of living organisms but could be present under pathological conditions - e.g., metabolic stress.

8 Bibliography

1. Luisi, P. L., Walde, P. & Oberholzer, T. Lipid vesicles as possible intermediates in the origin of life. *Curr. Opin. Colloid Interface Sci.* **4**, 33–39 (1999).

2. Nelson, D. L. & Cox, M. M. *Lehninger principles of biochemistry*. (W.H. Freeman and Company, 2008).

3. Singer, S. J. & Nicolson, G. L. The fluid mosaic model of the structure of cell membranes. *Science* **175**, 720–731 (1972).

4. Nicolson, G. L. The Fluid - Mosaic Model of Membrane Structure: Still relevant to understanding the structure, function and dynamics of biological membranes after more than 40 years. *Biochim. Biophys. Acta - Biomembr.* **1838**, 1451–1466 (2014).

5. NCNR - Brian Kirby. The cell membrane. Available at: https://www.ncnr.nist.gov/programs/reflect/rp/biology/cell_membrane.html. (Accessed: 11th March 2018)

6. Pollard, T. D., Earnshaw, W. C., Lippincott-Schwartz, J. & Johnson, G. Membrane Structure and Dynamics. in *Cell Biology* 227–239 (Elsevier, 2017).

7. Gounaris, K. & Barber, J. Monogalactosyldiacylglycerol: The most abundant polar lipid in nature. *Trends Biochem. Sci.* **8**, 378–381 (1983).

8. Kraft, M. L. Sphingolipid Organization in the Plasma Membrane and the Mechanisms That Influence It. *Front. Cell Dev. Biol.* **4**, 154 (2017).

9. Brodnitz, M. H. Autoxidation of Saturated Fatty Acids. A Review. *J. Agric. Food Chem.* **16**, 994–999 (1968).

10. Porter, N. A., Caldwell, S. E. & Mills, K. A. Mechanisms of free radical oxidation of unsaturated lipids. *Lipids* **30**, 277–290 (1995).

11. Pichler, H. & Emmerstorfer-Augustin, A. Modification of membrane lipid compositions in single-celled organisms – From basics to applications. *Methods* **147**, 50–65 (2018).

12. Zhao, J. *et al.* Phase studies of model biomembranes: Complex behavior of DSPC/DOPC/Cholesterol. *Biochim. Biophys. Acta - Biomembr.* **1768**, 2764–2776 (2007).

13. Fontanesi, F. Mitochondria: Structure and Role in Respiration. in *eLS* 1–13 (John Wiley & Sons, Ltd (Ed.), 2015). doi:10.1002/9780470015902.a0001380.pub2

14. Berg, J. M., Tymoczko, J. L. & Stryer, L. The light reactions of photosynthesis. in *Biochemistry* 1026 (W. H. Freeman and Company, 2002).

15. Dupuy, A. D. & Engelman, D. M. Protein area occupancy at the center of the red blood cell membrane. *Proc. Natl. Acad. Sci.* **105**, 2848–2852 (2008).

16. Guerrero-Valero, M. *et al.* Structural and mechanistic insights into the association of PKC -C2 domain to PtdIns(4,5)P2. *Proc. Natl. Acad. Sci.* **106**, 6603–6607 (2009).

17. Morales, K. A. *et al.* Pb2+ as modulator of protein-membrane interactions. *J. Am. Chem. Soc.* **133**, 10599–10611 (2011).

18. Dumas, J. J. *et al.* Multivalent endosome targeting by homodimeric EEA1. *Mol. Cell* **8**, 947–58 (2001).

19. Li, Q., Wong, Y. L. & Kang, C. Solution structure of the transmembrane domain of the insulin receptor in detergent micelles. *Biochim. Biophys. Acta - Biomembr.* **1838**, 1313–1321 (2014).

20. Chang, Y. *et al.* Structural basis for a pH-sensitive calcium leak across membranes. *Science (80-.).* **344**, 1131–1135 (2014).

21. Hutter, C. A. J. *et al.* Structure of the oligogalacturonate-specific KdgM porin. *Acta Crystallogr. Sect. D Biol. Crystallogr.* **70**, 1770–1778 (2014).

22. Almén, M. S., Nordström, K. J., Fredriksson, R. & Schiöth, H. B. Mapping the human membrane proteome: A majority of the human membrane proteins can be classified according to function and evolutionary origin. *BMC Biol.* **7**, 50 (2009).

23. Lin, S. H. & Guidotti, G. Purification of Membrane Proteins. in *Methods in Enzymology* **463**, 619–629 (Elsevier, 2009).

24. Olšinová, M. *et al.* Roughness of Transmembrane Helices Reduces Lipid Membrane Dynamics. *iScience* **10**, 87–97 (2018).

25. Ramadurai, S. *et al.* Lateral diffusion of membrane proteins. *J. Am. Chem. Soc.* **131**, 12650–12656 (2009).

26. De Planque, M. R. R. *et al.* Influence of lipid/peptide hydrophobic mismatch on the thickness of diacylphosphatidylcholine bilayers. A2H NMR and ESR study using designed transmembrane α-helical peptides and gramicidin A. *Biochemistry* **37**, 9333–9345 (1998).

27. Davis, J. H., Clare, D. M., Hodges, R. S. & Bloom, M. Interaction of a Synthetic Amphiphilic Polypeptide and Lipids in a Bilayer Structure. *Biochemistry* **22**, 5298–5305 (1983).

28. Kaiser, H.-J. *et al.* Lateral sorting in model membranes by cholesterol-mediated hydrophobic matching. *Proc. Natl. Acad. Sci. U. S. A.* **108**, 16628–16633 (2011).

29. Chan, Y.-H. M. & Boxer, S. G. Model Membrane Systems and Their Applications. *Curr. Opin. Chem. Biol.* **11**, 581 (2007).

30. Bernardino de la Serna, J., Schütz, G. J., Eggeling, C. & Cebecauer, M. There Is No Simple Model of the Plasma Membrane Organization. *Front. Cell Dev. Biol.* **4**, 106 (2016).

31. Veatch, S. L. & Keller, S. L. Separation of Liquid Phases in Giant Vesicles of Ternary Mixtures of Phospholipids and Cholesterol. *Biophys. J.* **85**, 3074–3083 (2003).

32. Cebecauer, M. *et al.* Membrane Lipid Nanodomains. *Chem. Rev.* **118**, 11259–11297 (2018).

33. Mouritsen, O. G. The liquid-ordered state comes of age. *Biochim. Biophys. Acta - Biomembr.* **1798**, 1286–1288 (2010).

34. Demchenko, A. P., Mély, Y., Duportail, G. & Klymchenko, A. S. Monitoring biophysical properties of lipid membranes by environment-sensitive fluorescent probes. *Biophys. J.* **96**, 3461–3470 (2009).

35. Mitra, K., Ubarretxena-Belandia, I., Taguchi, T., Warren, G. & Engelman, D. M. Modulation of the bilayer thickness of exocytic pathway membranes by membrane proteins rather than cholesterol. *Proc. Natl. Acad. Sci.* **101**, 4083–4088 (2004).

36. Killian, J. A. Synthetic peptides as models for intrinsic membrane proteins. *FEBS Lett.* **555**, 134–138 (2003).

37. Khandelia, H. & Mouristen, O. G. Lipid gynmastics: evidence of complete acyl chain reversal in oxidized phospholipids from molecular simulations. *Biophys. J.* **96**, 2734–2743 (2009).

38. Štefl, M. *et al.* Comprehensive portrait of cholesterol containing oxidized membrane. *Biochim. Biophys. Acta - Biomembr.* **1838**, 1769–1776 (2014).

39. Beranova, L., Cwiklik, L., Jurkiewicz, P., Hof, M. & Jungwirth, P. Oxidation changes physical properties of phospholipid bilayers: Fluorescence spectroscopy and molecular simulations. *Langmuir* **26**, 6140–6144 (2010).

40. Plochberger, B. *et al.* Cholesterol slows down the lateral mobility of an oxidized phospholipid in a supported lipid bilayer. *Langmuir* **26**, 17322–17329 (2010).

41. Schwarz, D. S. & Blower, M. D. The endoplasmic reticulum: Structure, function and response to cellular signaling. *Cellular and Molecular Life Sciences* **73**, 79–94 (2016).

42. Jan, C. H., Williams, C. C. & Weissman, J. S. Principles of ER cotranslational translocation revealed by proximity-specific ribosome profiling. *Science* **346**, 1257521 (2014).

43. Schuck, S., Prinz, W. A., Thorn, K. S., Voss, C. & Walter, P. Membrane expansion alleviates endoplasmic reticulum stress independently of the unfolded protein response. *J. Cell Biol.* **187**, 525–536 (2009).

44. Ron, D. & Walter, P. Signal integration in the endoplasmic reticulum unfolded protein response. *Nat. Rev. Mol. Cell Biol.* **8**, 519–529 (2007).

45. Mori, K. Signalling Pathways in the Unfolded Protein Response: Development from Yeast to Mammals. *J. Biochem.* **146**, 743–750 (2009).

46. Ye, J. *et al.* ER stress induces cleavage of membrane-bound ATF6 by the same proteases that process SREBPs. *Mol. Cell* **6**, 1355–1364 (2000).

47. Haze, K., Yoshida, H., Yanagi, H., Yura, T. & Mori, K. Mammalian Transcription Factor ATF6 Is Synthesized as a Transmembrane Protein and Activated by Proteolysis in Response to Endoplasmic Reticulum Stress. *Mol. Biol. Cell* **10**, 3787–3799 (1999).

48. Walter, P. & Ron, D. The Unfolded Protein Response: From Stress Pathway to Homeostatic Regulation. *Science (80-.).* **334**, 1081–1086 (2011).

49. Marciniak, S. J. *et al.* CHOP induces death by promoting protein synthesis and oxidation in the stressed endoplasmic reticulum. *Genes Dev.* **18**, 3066–3077 (2004).

50. Hu, H., Tian, M., Ding, C. & Yu, S. The C/EBP homologous protein (CHOP) transcription factor functions in endoplasmic reticulum stress-induced apoptosis and microbial infection. *Front. Immunol.* **9**, 3083 (2019).

51. Lin, J. H., Li, H., Zhang, Y., Ron, D. & Walter, P. Divergent effects of PERK and IRE1 signaling on cell viability. *PLoS One* **4**, e4170 (2009).

52. Nikawa, J. & Yamashita, S. IRE1 encodes a putative protein kinase containing a membrane-spanning domain and is required for inositol phototrophy in Saccharomyces cerevisiae. *Mol. Microbiol.* **6**, 1441–6 (1992).

53. Carman, G. M. & Han, G.-S. Regulation of Phospholipid Synthesis in the Yeast Saccharomyces cerevisiae. *Annu. Rev. Biochem.* **80**, 859–883 (2011).

54. Jonikas, M. C. *et al.* Comprehensive characterization of genes required for protein folding in the endoplasmic reticulum. *Science (80-.).* **323**, 1693–1697 (2009).

55. Pineau, L. *et al.* Lipid-induced ER stress: Synergistic effects of sterols and saturated fatty acids. *Traffic* **10**, 673–690 (2009).

56. Credle, J. J., Finer-Moore, J. S., Papa, F. R., Stroud, R. M. & Walter, P. On the mechanism of sensing unfolded protein in the endoplasmic reticulum. *Proc. Natl. Acad. Sci.* **102**, 18773–18784 (2005).

57. Promlek, T. *et al.* Membrane aberrancy and unfolded proteins activate the endoplasmic reticulum stress sensor Ire1 in different ways. *Mol. Biol. Cell* **22**, 3520–3532 (2011).

58. Volmer, R., van der Ploeg, K. & Ron, D. Membrane lipid saturation activates endoplasmic reticulum unfolded protein response transducers through their transmembrane domains. *Proc. Natl. Acad. Sci.* **110**, 4628–4633 (2013).

59. Volmer, R. & Ron, D. Lipid-dependent regulation of the unfolded protein response. *Curr. Opin. Cell Biol.* **33**, 67–73 (2015).

60. Kono, N., Amin-Wetzel, N. & Ron, D. Generic membrane-spanning features endow IRE1α with responsiveness to membrane aberrancy. *Mol. Biol. Cell* **28**, 2318–2332 (2017).

61. Halbleib, K. *et al.* Activation of the Unfolded Protein Response by Lipid Bilayer Stress. *Mol. Cell* **67**, 673–684 (2017).

62. Radanović, T., Reinhard, J., Ballweg, S., Pesek, K. & Ernst, R. An Emerging Group of Membrane Property Sensors Controls the Physical State of Organellar Membranes to Maintain Their Identity. *BioEssays* **40**, 1700250 (2018).

63. Hoppe, T. *et al.* Activation of a membrane-bound transcription factor by regulated ubiquitin/proteasome-dependent processing. *Chemtracts* **14**, 148–151 (2001).

64. Covino, R. *et al.* A Eukaryotic Sensor for Membrane Lipid Saturation. *Mol. Cell* **63**, 49–59 (2016).

65. De Kroon, A. I. P. M., Rijken, P. J. & De Smet, C. H. Checks and balances in membrane phospholipid class and acyl chain homeostasis, the yeast perspective. *Prog. Lipid Res.* **52**, 374–394 (2013).

66. Caffrey, M., Koynova, R., Hogan, J. & Moynihan, D. LIPIDAT: A Database of Lipid Phase Transition Temperatures, Enthalpy Changes, and Associated Information. in *Handbook of Nonmedical Applications of Liposomes* 86–104 (1996).

67. Weissman, A. M. *et al.* Molecular cloning and chromosomal localization of the human T-cell receptor zeta chain: distinction from the molecular CD3 complex. *Proc. Natl. Acad. Sci.* **85**, 9709–9713 (1988).

68. Berne, B. J. & Pecora, R. *Dynamic light scattering : with applications to chemistry, biology, and physics*. (Dover Publications, 2000).

69. Malvern Panalytical. *Dynamic light scattering: An introduction in 30 minutes. Tecnical note (MRK656-01)*. (2010).

70. René Albani, J. Fluorescence lifetimes of tryptophan: Structural origin and relation with s o → 1l b and s o → 1l a transitions. *J. Fluoresc.* **19**, 1061–1071 (2009).

71. Rasmussen, T. *et al.* Tryptophan in the Pore of the Mechanosensitive Channel MscS. *J. Biol. Chem.* **285**, 5377–5384 (2010).

72. Valeur, B. *Molecular Fluorescence: Principles and Applications*. (WILEY-VCH, 2002).

73. Wahl, M. *PicoQuant- Time-Correlated Single Photon Counting The Principle of Time-Correlated*. (2017).

74. Kapusta, P. *Time-resolved fluorescence anisotropy measurements made simple*. (2002).

75. Smith, T. A. & Ghiggino, K. P. A review of the analysis of complex time-resolved fluorescence anisotropy data. *Methods Appl. Fluoresc.* **3**, 022001 (2015).

76. Edelhoch, H. Spectroscopic Determination of Tryptophan and Tyrosine in Proteins. *Biochemistry* **6**, 1948–1954 (1967).

77. Birge, R. R. *Kodak Laser Dyes*. (Laboratory and Research Products Division, 1987).

78. Melcrová, A. *et al.* The complex nature of calcium cation interactions with phospholipid bilayers. *Sci. Rep.* **6**, 38035 (2016).

79. Bochkov, V. *et al.* Pleiotropic effects of oxidized phospholipids. *Free Radic. Biol. Med.* **111**, 6–24 (2017).

80. Hunter, D. G. & Frisken, B. J. Effect of extrusion pressure and lipid properties on the size and polydispersity of lipid vesicles. *Biophys. J.* **74**, 2996–3002 (1998).

81. Patty, P. J. & Frisken, B. J. The pressure-dependence of the size of extruded vesicles. *Biophys. J.* **85**, 996–1004 (2003).

82. Sabó, J. Mass spectrometry analysis of integral membrane peptides. (Charles University, 2018).

83. Lew, S., Caputo, G. A. & London, E. The effect of interactions involving ionizable residues flanking membrane-inserted hydrophobic helices upon helix-helix interaction. *Biochemistry* **42**, 10833–10842 (2003).

84. The UniProt Consortiom. UniProt: A worldwide hub of protein knowledge. *Nucleic Acids Res.* **47**, D506–D515 (2019).

85. Mouritsen, O. G. & Bloom, M. Mattress model of lipid-protein interactions in membranes. *Biophys. J.* **46**, 141–153 (1984).

86. Bogen, S.-T., de Korte-Kool, G., Lindblom, G. & Johansson, L. B.-Å. Aggregation of an α-Helical Transmembrane Peptide in Lipid Phases, Studied by Time-Resolved Fluorescence Spectroscopy. *J. Phys. Chem. B* **103**, 8344–8352 (1999).

87. Matalon, E. *et al.* Topology of the trans-membrane peptide WALP23 in model membranes under negative mismatch conditions. *J. Phys. Chem. B* **117**, 2280–2293 (2013).

88. Yang, L. *et al.* Oxidative and endoplasmic reticulum stresses are involved in palmitic acid-induced H9c2 cell apoptosis. *Biosci. Rep.* **39**, 1–9 (2019).

89. Itri, R., Junqueira, H. C., Mertins, O. & Baptista, M. S. Membrane changes under oxidative stress: The impact of oxidized lipids. *Biophys. Rev.* **6**, 47–61 (2014).

90. Parkkila, P., Štefl, M., Olzyńska, A., Hof, M. & Kinnunen, P. K. J. Phospholipid lateral diffusion in phosphatidylcholine-sphingomyelin-cholesterol monolayers; Effects of oxidatively truncated phosphatidylcholines. *Biochim. Biophys. Acta - Biomembr.* **1848**, 167–173 (2015).

91. Reis, A. & Spickett, C. M. Chemistry of phospholipid oxidation. *Biochim. Biophys. Acta - Biomembr.* **1818**, 2374–2387 (2012).

Svoluji k zapůjčení této práce pro studijní účely a prosím, aby byla řádně vedena evidence vypůjčovatelů.

Jméno a příjmení S adresou	Číslo OP	Datum vypůjčení	Poznámka